

## THE INITIAL MASS FUNCTION AND DISK FREQUENCY OF THE $\rho$ OPHIUCHI CLOUD: AN EXTINCTION-LIMITED SAMPLE

KRISTEN L. ERICKSON<sup>1,3</sup>, BRUCE A. WILKING<sup>1,3</sup>, MICHAEL R. MEYER<sup>2</sup>, JOHN G. ROBINSON<sup>1,4</sup>, AND LAUREN N. STEPHENSON<sup>1</sup>

<sup>1</sup> Department of Physics and Astronomy, University of Missouri-St. Louis, 1 University Boulevard, St. Louis, MO 63121, USA;

kle6x2@mail.umsl.edu, bwilking@umsl.edu, jrobinson@gmail.com, lnaфф@mail.umsl.edu

<sup>2</sup> Institute for Astronomy, Swiss Federal Institute of Technology, Wolfgang-Pauli-Strasse 27, CH-8093 Zurich, Switzerland; mmeyer@phys.ethz.ch

Received 2011 March 23; accepted 2011 August 15; published 2011 September 16

### ABSTRACT

We have completed an optical spectroscopic survey of an unbiased, extinction-limited sample of candidate young stars covering  $1.3 \text{ deg}^2$  of the  $\rho$  Ophiuchi star-forming region. While infrared, X-ray, and optical surveys of the cloud have identified many young stellar objects (YSOs), these surveys are biased toward particular stages of stellar evolution and are not optimal for studies of the disk frequency and initial mass function. We have obtained over 300 optical spectra to help identify 135 association members based on the presence of  $H\alpha$  in emission, lithium absorption, X-ray emission, a mid-infrared excess, a common proper motion, reflection nebosity, and/or extinction considerations. Spectral types along with  $R$ - and  $I$ -band photometry were used to derive effective temperatures and bolometric luminosities for association members to compare with theoretical tracks and isochrones for pre-main-sequence stars. An average age of 3.1 Myr is derived for this population which is intermediate between that of objects embedded in the cloud core of  $\rho$  Ophiuchi and low-mass stars in the Upper Scorpius subgroup. Consistent with this age we find a circumstellar disk frequency of  $27\% \pm 5\%$ . We also constructed an initial mass function for an extinction-limited sample of 123 YSOs ( $A_v \leq 8 \text{ mag}$ ), which is consistent with the field star initial mass function for YSOs with masses  $>0.2 M_\odot$ . There may be a deficit of brown dwarfs but this result relies on completeness corrections and requires confirmation.

*Key words:* ISM: individual objects ( $\rho$  Ophiuchi cloud) – open clusters and associations: individual (Upper Scorpius) – stars: formation – stars: pre-main sequence

*Online-only material:* color figure

### 1. INTRODUCTION

An important question in the theory of star formation is whether the initial mass function (IMF) of stars is universal. Variations in the IMF from region to region may hold clues to the roles of accretion, fragmentation, and ejection in producing the stellar mass spectrum (e.g., Bonnell et al. 2007). One of the best places to investigate the IMF is in molecular clouds with active star formation since cluster membership is well-determined, low-mass stars have had a limited amount of time to segregate, and one can associate variations in the IMF to the physical conditions of the cloud. Due to large columns of dust obscuring all but the brightest objects in the cloud, IMF studies of young clusters require unbiased, extinction-limited spectroscopic surveys (e.g., Bastian et al. 2010).

The  $\rho$  Ophiuchi molecular cloud complex is a well-studied, nearby region of active star formation (see Wilking et al. 2008 for review). Located at 130 pc from the Sun (Mamajek 2008), its proximity guarantees access to the broadest range of luminosity and mass. Most recently, the *Spitzer Space Telescope* surveyed  $\rho$  Ophiuchi in the mid- and far-infrared as part of the Legacy and guaranteed time programs. About 292 young stellar objects (YSOs) were identified with infrared excesses due to

circumstellar disks (Evans et al. 2009) over a field of view of  $6.8 \text{ deg}^2$ . X-ray studies have also been conducted of the region with *ROSAT*, *XMM-Newton*, *ASCA*, and *Chandra* revealing more evolved YSOs with magnetic surface activity (Grosso et al. 2000; Gagné et al. 2004; Ozawa et al. 2005). But for studies of the IMF, one must sample all phases of pre-main-sequence (PMS) evolution from heavily embedded YSOs in their main accretion phase, to classical T Tauri stars (CTTS), to weak-emission T Tauri stars (WTTS) with little or no circumstellar dust. Optical spectroscopic surveys targeting CTTS and WTTS have been conducted of this region, however these studies have been biased toward objects with X-ray emission or YSOs with suspected  $H\alpha$  emission (Bouvier & Appenzeller 1992; Martín et al. 1998; Wilking et al. 2005). Wilking et al. (2005, hereafter Paper I) obtained 136 spectra from  $5820 \text{ \AA}$  to  $8700 \text{ \AA}$  at a resolution of  $2.9 \text{ \AA}$  and identified 88 cluster members in the main L 1688 cloud of the Ophiuchus complex. The members had a median age of 2.1 Myr and included 39 CTTS. However, their survey had a selection bias toward YSOs with  $H\alpha$  emission.

In this paper, we present the results of a new optical spectroscopic survey which, when combined with data from Paper I, enables us to construct an unbiased, extinction-limited sample of YSOs in the L 1688 cloud. Section 2 describes this new spectroscopic survey which covered the wavelength range  $6249\text{--}7657 \text{ \AA}$  with a resolution of  $1.4 \text{ \AA}$  that enabled us to resolve Li in absorption, an indicator of youth. The analysis of the spectra to derive spectral types and exclude background giants is described briefly in Section 3. Section 4 discusses the results of our analysis including the identification of association members, their spatial distribution, their placement in a Hertzsprung–Russell (H-R) diagram relative to several

<sup>3</sup> Visiting Astronomer, Kitt Peak National Observatory, National Optical Astronomy Observatory, which is operated by the Association of Universities for Research in Astronomy (AURA) under cooperative agreement with the National Science Foundation.

<sup>4</sup> Visiting Astronomer, Cerro Tololo Inter-American Observatory, National Optical Astronomy Observatory, which are operated by the Association of Universities for Research in Astronomy, under contract with the National Science Foundation.

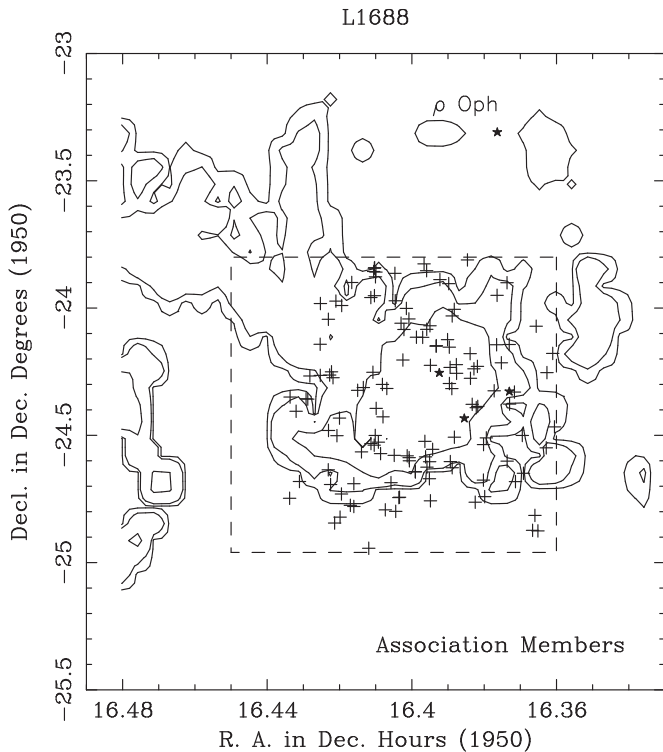


**Figure 1.** Distribution of association members is shown relative to contours of  $^{13}\text{CO}$  column density. The contours were computed from Loren (1989) assuming LTE and  $T_{\text{ex}} = 25$  K. The values of the contours in units of  $\text{cm}^{-2}$  are  $6 \times 10^{14}$ ,  $3 \times 10^{15}$ , and  $1.5 \times 10^{16}$ ; the lowest contour delineates the outer boundary of the dark cloud. The dashed box outlines the field included by our Hydra observations. Star symbols mark the locations of the star  $\rho$  Oph A (labeled) and the association members Oph S1, SR 3, and HD 147889 in the L 1688 core.

theoretical models and their age distribution. The section concludes by defining an extinction-limited sample and the resulting disk frequency and distribution of masses in this subsample for comparisons with other star-forming regions. Finally, Section 5 compares low-extinction YSOs in L 1688 with those in Upper Scorpius and explores the relationship between star formation in Upper Scorpius, the surface population in L 1688, and that in the cloud core.

## 2. OBSERVATIONS AND DATA REDUCTION

Over 200 moderate resolution spectra were obtained for 184 stars identified through  $R$ - and  $I$ -band photometry as candidate YSOs. Fifty-two of these stars had spectral classifications reported in Paper I, allowing us to refine our previous spectral classifications. Newly observed YSO candidates numbered 133. These observations are described in detail in the following sections.

### 2.1. Sample Selection

Candidate YSOs were selected from an  $I$  versus  $(R - I)$  color-magnitude diagram.  $R$ - and  $I$ -band photometry were obtained from short (5 minute) exposure images obtained with the 0.6 m Curtis-Schmidt Telescope located at Cerro Tololo Inter-American Observatory in 1995 March (see also Wilking et al. 1997 for description). The CCD images covered a  $67' \times 68.5'$  area centered on  $\text{R.A.}(2000) = 16^{\text{h}}27^{\text{m}}14^{\text{s}}$ ,  $\text{decl.}(2000) = -24^{\circ}30'06''$  with a scale of  $2''.03 \text{ pixel}^{-1}$ . The survey area is shown in Figure 1 relative to the distribution of molecular gas. Photometry was performed using an  $8''1$

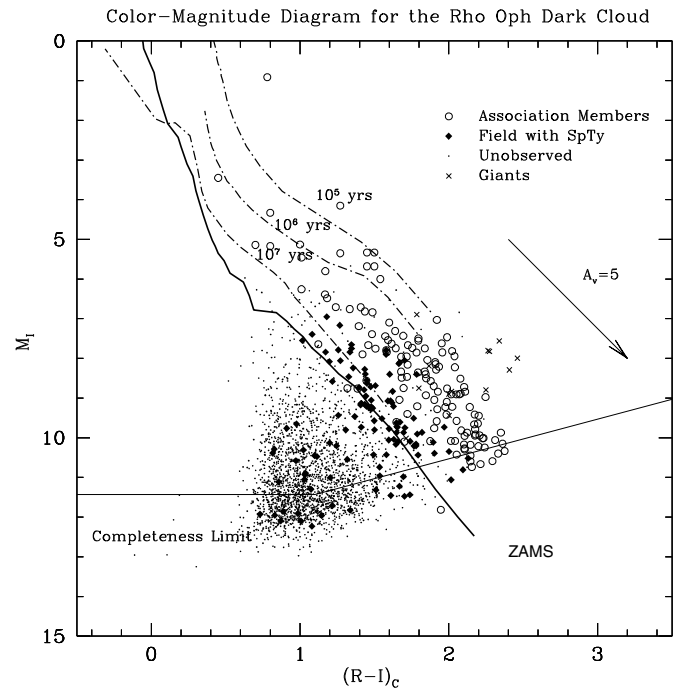


**Figure 2.**  $I$  vs.  $(R - I)$  color-magnitude diagram from our  $R$ - and  $I$ -band images. The ordinate is the absolute  $I$  magnitude assuming a distance of 130 pc and with no correction for reddening. Objects observed spectroscopically are shown by open circles (association members), diamonds (field stars), or “x”s (giants). Isochrones and the ZAMS from the DM models are shown for comparison.

diameter aperture optimized for the  $4''$  full width at half-maximum of the point-spread function (Howell 1989) with local sky background measured in an annulus  $10'' - 20''$  in diameter. Zero points were computed in the Kron-Cousins photometric system using standard star fields established by Landolt (1992). Completeness limits were estimated by adding artificial stars in half magnitude intervals to the images and extracting them using DAOFIND in the Image Reduction and Analysis Facility (IRAF).<sup>5</sup> Recovery of  $\geq 90\%$  of the artificial stars occurred for  $R \leq 18.1$  mag and  $I \leq 17.0$  mag. Photometry was not reliable for stars with  $R \leq 12.4$  mag and  $I \leq 11.8$  due to saturation of the CCD.

An  $I$  versus  $(R - I)$  diagram for over 2500 stars is presented in Figure 2. The ordinate is the absolute  $I$  magnitude assuming a distance of 130 pc. For stars saturated in our images,  $R$ - and  $I$ -band photometry was adopted from the studies of Chini (1981), S. Gordon and K. M. Strom (1990, unpublished data), Bouvier & Appenzeller (1992), or Walter et al. (1994). Photometry from Chini was transformed into the Kron-Cousins system using the relations derived by Fernie (1983). The diagram is complete for the brightest stars which are candidate YSOs except for RXJ 1624.9-2459, ROXR1-4/SR-8, SR 24n, HD 148352, and ROXR2-15 for which previous photometry was not available. For comparison, PMS isochrones and the zero-age main sequence (ZAMS) derived from the models of D’Antona & Mazzitelli (1997) are shown (see Section 4.4). One of the known association members, WL 18, has strong  $\text{H}\alpha$  emission ( $\text{EW} = 96 \text{ \AA}$ ) relative to the  $R$ -band continuum which may explain its position below the ZAMS.

<sup>5</sup> IRAF is distributed by the National Optical Astronomy Observatory, which is operated by the Association of Universities for Research in Astronomy, Inc., under cooperative agreement with the National Science Foundation.

**Table 1**  
Summary of Hydra Observations

Field No.	Date (YYMMDD)	Telescope	Position (J2000.0)	Sources	No. of Exp.	Int. Time (minutes)
1	030810	Blanco	16:27:05.4–24:45:09	24	5	135
2	030811	Blanco	16:28:15.2–24:14:04	47	5	135
3	030812	Blanco	16:26:01.9–24:14:23	48	5	135
4	060615	WIYN	16:25:47.2–24:41:00	32	10	240
5	060616	WIYN	16:28:21.6–24:28:00	42	10	240
6	060617	WIYN	16:27:22.9–24:09:00	30	10	240

From this diagram, we have drawn a sample for spectroscopic follow-up of stars which are on or above the  $10^7$  yr isochrone and brighter than our completeness limits. Samples selected from this region of the color–magnitude diagram should be representative for stars earlier than M6 with  $A_v \leq 3$  mag and ages  $\leq 10^7$  yr.

Accurate positions ( $<0''.5$ ) for these stars were obtained using the ASTROM program distributed by the Starlink Project and a set of secondary astrometric standards. The secondary position references were 27 H $\alpha$  emission-line stars with accurate positions determined relative to SAO stars in a 5 deg<sup>2</sup> region on the Red Palomar Sky Survey plate (Wilking et al. 1987). These positions were compared to counterparts from the Two Micron All Sky Survey (2MASS); matches were found within a radius of 2''. Positions were then shifted by +0.2 s in right ascension to bring them into agreement with the 2MASS coordinate system (Cutri et al. 2003).

### 2.2. Hydra Observations

Optical spectra were obtained for stars located over a 1.3 deg<sup>2</sup> area centered on L 1688 using Hydra, the multi-fiber spectrograph, on two different telescopes. Fiber configurations were designed to observe the maximum number of candidate YSOs; crowding at the edges of our field restricted the number of sources that could be observed. The first set of observations were made using Hydra on the Blanco 4 m telescope at Cerro Tololo Inter-American Observatory on 2003 August 10–12. The Bench Schmidt camera with the SiTe 2k  $\times$  4k CCD gave a 40' field of view. The fibers (2'' diameter) coupled with the 790 lines mm<sup>-1</sup> KPGLD grating yielded a wavelength coverage of 6275–7975 Å centered near 7125 Å. The spectral dispersion was 0.90 Å pixel<sup>-1</sup> giving an effective resolution of 2.7 Å. The resolution at the central wavelength was  $\lambda/\Delta\lambda = 2600$ . The second set of observations utilized Hydra on the WIYN<sup>6</sup> 3.5 m telescope on 2006 June 15–17. The Bench Spectrograph Camera was used with the T2KA CCD which gave a 1° field of view. The red fiber cable (2'' diameter) and the 1200 lines mm<sup>-1</sup> grating with a blaze angle of 28:7 were combined with the GG-495 filter to cover the range of 6250–7657 Å centered near 6960 Å. The spectral dispersion was 0.68 Å pixel<sup>-1</sup> giving an effective resolution of 1.4 Å. The resolution at the central wavelength was  $\lambda/\Delta\lambda = 5000$ . Three fiber configurations were observed at each telescope, set to observe overlapping regions of the 1.3 deg<sup>2</sup> target field.

The spectra were reduced using IRAF. Images were processed for bias and dark corrections using CCDPROC. Multiple exposures of a given field were median-combined and then reduced

with IRAF's DOHYDRA package. The images were flat-fielded using dome flats obtained for each fiber configuration. Sky subtraction was accomplished using the median of 7–10 sky spectra distributed across the field for each configuration. The spectra were wavelength calibrated using 5 s exposures of the PENRAY (CTIO: He, Ne, Ar, Xe) or CuAr (WIYN) lamps taken in each fiber configuration. Scattered light corrections were not made and no flux calibration was performed. In Table 1, we summarize the observations by presenting for each field the observation date and telescope, pointing center, number of candidate YSOs observed, number of exposures, and the total integration time. The typical signal-to-noise ratio for stars with  $R = 16$  mag was 30 for the CTIO spectra and 20 for the WIYN spectra as measured by line free regions of the continuum.

### 3. ANALYSIS OF THE SPECTRA

As in Paper I, spectral types were derived from visual classification (visual pattern matching of our smoothed program star spectra with standard star spectra) supported by quantitative analysis of some spectral indices. For the purposes of matching spectral features with those of standard stars, our Hydra spectra were smoothed using a Gaussian filter to the resolution of the standard stars used for direct comparison. All spectra have been normalized to 1 by dividing out a fit to the continua, carefully excluding regions with emission lines or broad absorption due to TiO. Normalized spectra were smoothed to a resolution of 5.7 Å for comparison with the spectral standards of Allen & Strom (1995). For giants and later type dwarfs (M5V–M9V), optical spectra from the study of Kirkpatrick et al. (1991) were used with an effective resolution of either 8 or 18 Å. The relative strength of absorption due to H $\alpha$  and a blend of Ba II, Fe I, and Ca I centered at 6497 Å is the most sensitive indicator of spectral type for F-K stars and the depth of the TiO bands for K-M stars.

A rough estimate of the surface gravity of an object is important in distinguishing PMS stars from background giants. The primary gravity-sensitive absorption feature available for analysis in our spectra was the CaH band centered at 6975 Å. This band is evident in the spectra of dwarf stars with spectral types later than K5. Following Allen (1996), we have calculated a CaH index as the ratio of the continuum at  $7035 \pm 15$  Å to the flux in the CaH absorption band at  $6975 \pm 15$  Å and a TiO index (primarily temperature sensitive for stars  $\geq$  K5) as the ratio of the continuum at  $7030 \pm 15$  Å to the flux in the TiO absorption band at  $7140 \pm 15$  Å from the unsmoothed, normalized spectrum of each program object. In Figure 3, we plot the CaH index versus TiO index for 136 program objects. Error bars are computed based on the  $1\sigma$  error in the mean in flux averages and propagated to the ratios. The solid lines represent first- or second-order fits to the standard star spectra.

<sup>6</sup> The WIYN Observatory is a joint facility of the University of Wisconsin-Madison, Indiana University, Yale University, and the National Optical Astronomy Observatory.

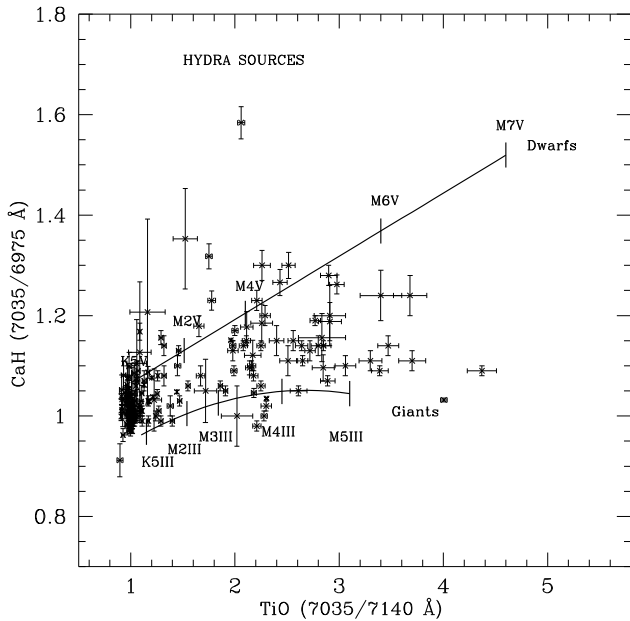


**Figure 3.** Plot of the CaH vs. TiO indices as defined in the text for 136 program objects. The solid lines were derived from fits to dwarf and giant spectral standards. For the dwarf standards from K5–M7, the fit was  $y = 0.126x + 0.940$  with a correlation coefficient of  $r = 0.94$ . We note that for spectral types later than M7, both indices decrease in response to an overall depression of the continuum so that an M8 V star has a CaH index similar to that of an M4 V star. For the giant standards from K5–M5, the fit gave  $y = -0.0357x^2 + 0.191x + 0.795$  with a correlation coefficient of  $r = 0.82$ .

#### 4. RESULTS

Spectral types were determined for 174 of 184 stars in this study. These data are presented in Table 2 along with any previous source names, X-ray associations, R.A. and decl. in J2000, the  $(R-I)$  color indices,  $I$  magnitudes, and previous spectral classifications. The presence of lithium absorption at  $6707 \text{ \AA}$  and the equivalent width of  $H\alpha$  are also given (emission shown as a negative value). Based on the CaH index, we have identified nine background giants and seven possible dwarfs. Spectral classifications agree well with optical and infrared spectral types previously published by Bouvier & Appenzeller (1992), Martín et al. (1998), Luhman & Rieke (1999), Cieza et al. (2010), as well as those in Paper I. A notable exception is WLY 2-48/ISO-Oph 159. Geers et al. (2007) report an optical spectral type of M0 while Luhman & Rieke (1999) classify it as earlier than F3. Our spectrum shows broad  $H\alpha$  absorption partially filled in with emission as well as an absorption line from O I at  $7774 \text{ \AA}$  characteristic of early-type stars. The strength of the latter plus the absence of an absorption line due to the blend at  $6497 \text{ \AA}$  (Ba II, Fe I, Ca I) leads us to a spectral classification of A0. This spectral classification is in agreement with that derived by McClure et al. (2010).

When combined with the results of Paper I, optical spectra have been obtained for 87% of the stars in the  $M(I)$  versus  $(R-I)$  diagram that fell above our completeness limit and on or above the  $10^7$  year old isochrone. A reanalysis of the  $R$ - and  $I$ -band photometry has led us to revise some of the magnitudes published in Paper I. The revised photometry is presented in Table 4 in the Appendix and used to derive the stellar parameters in this paper.

##### 4.1. Emission-line Spectra

In our previous study, 39 of 131 sources (30%) were found to have strong  $H\alpha$  emission characteristic of CTTS. In this sample,

which was not biased toward the detection of  $H\alpha$  emission, 15 sources were found to have  $EW(H\alpha) > 10 \text{ \AA}$ . All of these are newly identified CTTS using this coarse criterion (Herbig & Bell 1988). An additional 17 objects showed weaker  $H\alpha$  emission ( $10 \text{ \AA} > EW(H\alpha) > 5 \text{ \AA}$ ) with all but one having an M spectral type. The variable nature of  $H\alpha$  emission is evident when comparing stars observed days apart and stars observed in this study and in Paper I.

##### 4.2. Identification of Pre-main-sequence Association Members

Identification of 35 new PMS objects was accomplished using the same membership criteria as in Paper I with some additional criteria as described below. An additional 13 YSOs with optical spectral types were taken from the literature. Combined with the 87 association members from Paper I, there are a total of 135 objects with optical spectral types that meet one or more of these criteria. These objects are listed in Table 3.<sup>7</sup> Ninety percent of the YSOs in our sample have K or M spectral types. The criteria include the following.

1.  $H\alpha$  in emission with  $EW > 10 \text{ \AA}$  during at least one observation, characteristic of CTTSs. Fifty-three objects fit this criterion.
2. Association with X-ray emission is a signpost of youth and has been observed in 82 stars in our sample.
3. The presence of lithium absorption is an indicator of youth for stars with spectral type K0 and cooler and clearly resolved in the spectra of 46 stars.
4. A mid-infrared excess as observed by the *Infrared Space Observatory (ISO)* with a spectral index from 2.2 to  $14 \mu\text{m}$  (Bontemps et al. 2001) or the *Spitzer Space Telescope* from 3.6 to  $24 \mu\text{m}$  (Wilking et al. 2008) indicative of a circumstellar disk. Thirty-eight objects display a mid-infrared excess.
5. A proper motion in common with the association mean as noted by Mamajek (2008). In addition, we include Object 1-3 from this study as a common proper motion member based on data from the UCAC3 catalog.
6. Two early-type stars, HD 147889 and Source 1, are associated with reflection nebulosity in the  $R$ - and  $I$ -band images.
7. Finally, 100 objects (excluding giants identified in Section 3) that are too luminous to be main-sequence objects at the distance to  $\rho$  Oph and have an estimate for  $A_v$  too high to be foreground to the cloud ( $A_v > 1.5$  mag).

We have noted in Table 3 objects with near-infrared variability from the study of Alves de Oliveira & Casali (2008) but do not require this for association membership. Only one of the objects classified as a possible dwarf based on the CaH index, Object 4-52, displayed a criterion for association membership, and is included in Table 3.

Mamajek (2008) has noted that proper motion data for two of the objects in Table 3, X-ray sources GY 280 and HD 148352, are discordant and are possible foreground objects. Despite this fact, we include them in Table 3 but note that X-ray emission alone may not be sufficient for identifying YSOs.

##### 4.3. Distribution of Association Members

The distribution of the 135 association members identified by this study is shown in Figure 1 relative to contours of  $^{13}\text{CO}$  column density which delineate the cloud boundaries (Loren

<sup>7</sup> One object, [WMR2005] 3-17, was removed as an association member from Paper I since one could not rule out that it is a background giant.

**Table 2**  
Optical Properties of Candidate Young Stellar Objects

<i>F</i>	Ap. <sup>a</sup>	Name(s) <sup>b</sup>	X-Ray ID <sup>c</sup>	R.A.(J2000) (hhmmss.s)	Decl.(J2000) (° ' ")	Li?	EW(H $\alpha$ )	<i>I</i>	( <i>R</i> − <i>I</i> ) <sup>d</sup> (mag)	Prev Sp. Ty. <sup>e</sup> (mag)	Sp. Ty.	Adopt	Notes
3	39			16 24 39.3	−24 07 10	...	1.1	15.31	1.41	...	K0-K2	K1	
4	40			16 24 39.7	−24 35 08	...	−9.2	15.87	2.11	...	M4.5	M4.5	
4	13			16 24 40.5	−24 43 09	...	<0.3	15.96	1.90	...	G5-K6	K0:	
3	11			16 24 40.7	−24 21 40	...	0.90	14.83	1.49	...	K0-K2	K1	
4	29			16 24 41.1	−24 17 49	...	> −0.4	15.15	2.05	...	M1-M3	M2	
4	99			16 24 43.9	−24 47 53	...	0.70	14.64	1.61	...	K3	K3	
4	14			16 24 44.8	−25 00 18	...	−3.5	15.74	1.64	...	M2-M4	M2	Poss. dwarf
3	37			16 24 46.9	−24 22 21	...	0.90	13.61	1.86	...	K6-M0	K7	
4	72			16 24 46.9	−24 22 02	...	<0.8	13.70	1.66	...	K2-K5	K4	
4	2	UCAC3		16 24 47.7	−24 52 58	...	1.0	13.41	1.17	...	G2-G5	G5	
4	42			16 24 48.1	−24 40 04	...	> −0.4	14.80	2.14	...	M3.5-M7	M4.5	
4	85			16 24 49.3	−24 28 12	...	1.0	14.20	1.45	...	K0-K5	K3:	
4	10			16 24 50.2	−24 35 39	...	1.3	15.39	1.66	...	G5-K5	U	
3	4			16 24 51.6	−24 17 21	...	0.9	14.69	1.62	...	K1-K3	K2	
3	12			16 24 55.7	−24 09 15	...	2.0	15.01	1.26	...	G2-G5	G4	
4	90	UCAC3		16 24 55.8	−24 53 34	...	1.1	...	...	...	K3-K6	K6	
3	58			16 24 57.3	−24 11 23	Yes	−3.0	13.72	1.91	M3.5 (WMR)	M3-M4	M3.5	
4	59	WSB 18		16 24 59.7	−24 55 59	Yes:	−87	13.78	1.93	...	M2.5-M4.5	M3.5	
4	82	WSB 19/UCAC3		16 25 02.0	−24 59 30	...	−40	13.12	1.80	...	M3-M5.5	M4.5	
3	28			16 25 03.8	−24 22 24	...	2.5	14.64	1.59	...	F6-G4	G0	
4	88	UCAC3		16 25 05.0	−24 41 09	...	0.80	13.47	1.58	...	K3-K5	K4	
3	42			16 25 05.6	−24 03 11	...	0.90	15.58	1.71	...	K6-M0	K7III	Giant
3	14			16 25 07.2	−23 59 48	...	3.7	16.04	1.11	...	F2-F5	F3	
3	44			16 25 07.9	−23 58 03	...	1.2	14.78	1.45	...	G5-K0	G9	
4	38			16 25 10.9	−24 46 03	...	−10	15.78	2.20	...	M4-M6	M5	
4	32			16 25 11.9	−24 37 07	...	0.80	14.78	1.79	...	K5-K6	K6	
3	31			16 25 12.3	−23 58 31	...	0.80	14.71	1.41	...	K1-K3	K2	
3	17			16 25 16.8	−24 04 41	...	0.80	15.37	1.50	...	K3	K3	
3	27			16 25 17.0	−24 11 44	...	0.80	14.36	2.25	...	M3-M4.5	M4.5III	Giant
4	52			16 25 18.9	−24 47 59	Yes:	−12	14.98	2.17	...	M2-M4	M3	Poss. dwarf
4	91	UCAC3		16 25 22.9	−24 57 18	...	0.70	12.74	1.27	...	K3-K5	K3	
4	26			16 25 23.1	−24 42 08	...	0.95	14.79	1.46	...	K1-K5	K3	
3	6			16 25 23.6	−24 22 54	...	1.6	15.61	1.63	...	G4-G9	G5	
3	35			16 25 24.1	−23 56 56	...	−1.6	15.18	1.67	M3 (WMR)	M3-M4	M3.5	Poss. dwarf
3	34			16 25 25.6	−24 07 28	...	1.2	15.19	1.65	...	G9-K0	K0	
6	42	Same as 3-34				...	<2			...	G5-K5		
3	30			16 25 26.3	−24 23 56	...	1.3	15.67	1.66	...	G5-K0	G7	
3	45			16 25 26.3	−24 01 06	...	0.90	14.50	1.85	...	K7-M0	K7	
3	3	UCAC3		16 25 26.7	−23 56 53	...	0.90	14.28	1.48	...	K0-K2	K2	
3	2			16 25 27.0	−24 20 50	...	0.70	15.66	1.74	...	K3-K4	K4	

Table 2  
(Continued)

<i>F</i>	Ap. <sup>a</sup>	Name(s) <sup>b</sup>	X-Ray ID <sup>c</sup>	R.A.(J2000) (hhmmss.s)	Decl.(J2000) (° ' ")	Li?	EW(H $\alpha$ )	<i>I</i>	( <i>R-I</i> ) <sup>d</sup> (mag)	Prev Sp. Ty. <sup>e</sup> (mag)	Sp. Ty.	Adopt	Notes
6	76			16 25 28.8	-24 22 59	...	<0.1	15.14	1.51	M3.25 (WMR)	U	M3.25	
4	65	UCAC3		16 25 29.9	-24 39 14	...	-0.30	14.15	1.22	M2 (WMR)	M1-M3	M2	Poss. dwarf
4	62			16 25 31.6	-24 21 22	...	<0.2	17.03	1.61	K1.5 (WMR)	<M0	K1.5	
4	17			16 25 32.3	-24 19 59	...	> -3.5	15.63	1.60	...	K7-M3	M0	
4	58			16 25 34.1	-24 36 32	...	<0.5	14.81	1.45	...	U	U	
3	50	GSS 15		16 25 35.6	-24 34 00	...	0.80	13.39	2.27	...	M3-M4.5	M4III	Giant
4	98	UCAC3		16 25 36.1	-25 00 26	...	> -0.2	13.65	1.20	...	K2-K6	K5	
3	5			16 25 36.2	-24 04 04	...	0.90	15.15	1.92	...	K5.5-K8	K6:	
3	56	ISO-Oph 1/WLY 2-2/UCAC3		16 25 36.8	-24 15 42	Yes	-2.8	13.36	1.58	K3.5 (LR)	K3-K5	K4	
3	49			16 25 37.8	-24 13 43	...	<0.2	13.57	2.46	M4.25III (WMR)	M3.5-M5	M4.25III	Giant
1	29			16 25 37.9	-24 43 05	...	0.70	14.71	1.41	...	K2-K4	K3	
3	40			16 25 44.2	-24 33 02	...	> -0.5	16.09	2.13	...	K2-K4	K3	
4	16	UCAC3	ROX3	16 25 49.6	-24 51 30	Yes	-2.4	11.03	1.01	K3/M0 (BA)	K6-M1	K8	
1	3	UCAC3		16 25 50.5	-24 47 34	...	1.0	13.47	1.42	...	G9-K0	K0	
1	28			16 25 51.0	-24 34 55	...	<0.2	16.38	2.10	...	K4	K4	
4	44	Same as 1-28				...	> -0.4			...	<K6		
6	5			16 25 52.5	-24 04 19	Yes:	0.70	16.02	1.10	F9.5 (WMR)	G5-K5	G9	
1	33			16 25 57.5	-24 42 07	...	1.0	14.40	1.62	...	K0-K2	K2	
1	15			16 25 57.6	-24 41 00	...	0.70	15.34	1.60	...	K0-K2	K1	
1	16			16 25 58.9	-24 52 47	Yes:	-7.3	13.86	1.92	M4.5 (WMR)	M2-M4	M4	
3	9			16 26 02.2	-24 02 04	...	0.60	13.76	1.87	...	M2.5-M4	M3III	Giant
3	53			16 26 03.0	-24 08 48	...	3.7	14.73	1.44	...	F2-F4	F3	
3	20	UCAC3		16 26 09.1	-24 01 29	...	1.0	13.81	1.36	...	K0-K3	K2	
4	11	UCAC3		16 26 10.9	-24 52 14	...	1.0	12.52	1.18	...	G9-K3	K1	
3	10	UCAC3		16 26 16.9	-24 00 07	...	1.0	13.36	1.26	...	K0-K3	K2	
3	43	GSS 29	ROXC J162616.8-242224	16 26 16.9	-24 22 23	Yes:	-2.6	15.23	2.17	K6 (LR)	K5-K6	K6	
4	93	Same as 3-43				Yes	> -2.5			...	K5-K6		
6	2	Same as 3-43				Yes	-0.50			...	K6		
3	15	UCAC3	RXJ1626.3-2407?	16 26 18.7	-24 07 19	Yes	-3.0	13.07	1.80	M3.25 (WMR)	M3-M3.5	M3.25	
3	29			16 26 18.8	-24 12 25	...	1.1	15.44	1.82	...	K1-K3	K2	
6	39			16 26 22.5	-23 58 19	...	> -1.0	16.12	1.32	K4 (WMR)	K6	K6	
3	23	GSS 32/Source 2	ROXC J162624.0-242449	16 26 24.1	-24 24 48	...	-7.6	15.58	2.23	K8 (LR)	K5-K6	K5	
3	51			16 26 24.3	-24 01 16	...	-11	15.84	2.11	M4.5 (WMR)	M3-M5.5	M4.5	
4	31			16 26 29.2	-24 48 15	...	1.3	16.46	1.04	G0 (WMR)	F6-G3	G0	
1	25			16 26 35.5	-24 55 58	...	> -0.4	16.00	1.58	...	K1-K3	K3	
3	16	ISO-Oph 51	ROXC J162636.8-241552	16 26 37.0	-24 15 52	Yes:	-9.6	15.67	1.70	...	K7-M1	M0	
3	26	AOC 88		16 26 37.5	-24 08 42	...	0.80	16.01	1.79	...	K2-K4	K3	
3	18	GSS 37/VSSG 2	ROXC J162642.8-242030	16 26 42.9	-24 20 30	...	-10	14.33	1.99	K6 (MMGC), M0 (LR)	K7-M2	M1	
3	33	UCAC3	ROXC J162643.2-241109	16 26 43.1	-24 11 09	Yes	-1.0	13.32	1.51	K8 (WMR)	K7-M0	K8	
1	21			16 26 43.5	-24 52 23	...	0.80	14.33	1.39	...	K6-K7	K6	

Table 2  
(Continued)

<i>F</i>	Ap. <sup>a</sup>	Name(s) <sup>b</sup>	X-Ray ID <sup>c</sup>	R.A.(J2000) (hhmmss.s)	Decl.(J2000) ( <sup>o</sup> ' ")	Li?	EW(H $\alpha$ )	<i>I</i>	( <i>R</i> − <i>I</i> ) <sup>d</sup> (mag)	Prev Sp. Ty. <sup>e</sup> (mag)	Sp. Ty.	Adopt	Notes
1	22		ROXN 6	16 26 44.4	−24 47 13	Yes	−4.0	13.92	1.79	M4.5 (WMR)	M3-M4	M4	
3	36			16 26 46.1	−23 58 10	...	−3.8	15.53	2.11	M3 (WMR)	M2-M4	M3	
1	8		ROXN 9	16 26 48.2	−24 42 03	...	−9.1	15.58	2.23	M3.75 (WMR)	M5-M6	M5	
4	34	Same as 1-8				...	−3.4				M4-M6		
2	56	AOC 64		16 26 50.5	−24 13 52	Yes	−6.2	14.79	2.02	M4.5 (WMR)	M3-M4	M3.5	
3	21	Same as 2-56				Yes	−5.8				M3-M4		
6	10			16 26 53.2	−24 05 58	...	> −0.4	16.92	1.48	K0.5 (WMR)	U	K0.5	
3	24			16 26 53.7	−24 01 55	...	1.6	15.78	1.77	...	G5-K2	G9	
6	85	Same as 3-24				...	> −3.0				U		
2	60	UCAC3		16 26 55.0	−24 10 16	...	0.2	13.84	1.44	M3 (WMR)	M2-M4	M3	
1	1			16 26 57.4	−24 49 48	...	0.70	15.78	1.78	...	K4-K5	K5	
4	4			16 26 57.8	−24 52 37	...	<0.5	17.48	0.98	K5 (WMR)	G2-K6	K5	
2	32		ROXC J162704.0-240932	16 27 04.2	−24 09 32	Yes	−4.1	14.06	1.68	M2 (MMGC)	M0-M2	M1	
3	7	Same as 2-32				Yes	−5.2				M0-M2		
2	51			16 27 04.5	−24 03 28	...	0.90	13.97	1.60	...	K0-K3	K2.5	
3	41	Same as 2-51				...	0.90				K1-K3		
1	5	ISO-Oph 97/GY 194	ROXRF 9	16 27 04.6	−24 42 13	Yes:	−2.6	15.66	1.88	...	K8-M0	M0	
5	67			16 27 04.6	−24 42 58	Yes	−3.5	14.97	1.72	...	K6-M1	K8	
2	29			16 27 06.6	−24 07 03	...	−4.3	15.36	2.18	M4.5 (WMR)	M3-M5	M4.5	
3	46	Same as 2-29				...	−12				M3-M5.5		
3	57	ISO-Oph 106		16 27 09.1	−24 12 01	...	−12	16.16	2.29	M2.5 (WMR)	U	M2.5	Poss. dwarf
5	81	Same as 3-57				...	−5.0				M2-M3		
2	23		ROXC J162711.8-241031	16 27 12.0	−24 10 31	Yes	−0.50	15.33	1.90	M0: (MMGC)	K4-K5	K6	
3	54	Same as 2-23				Yes:	> −1.5				K4-K6		
5	58	Same as 2-23				Yes	> −1.0				K6-M2		
6	38	Same as 2-23				...	−1.7				K6		
1	6	WSB 47		16 27 17.0	−24 47 11	...	0.70	15.08	1.76	K1 (WMR)	K2-K5	K2	
5	14	Same as 1-6				...	0.70				K4-K6		
2	61	UCAC3		16 27 17.1	−24 06 48	...	0.90	13.67	1.67	...	K1-K3	K3	
3	22	Same as 2-61				...	0.80				K2-K3		
6	62			16 27 18.0	−23 58 46	...	0.80	13.20	1.62	...	K7-K8	K8	
5	82			16 27 18.1	−24 53 16	...	−9.0	16.63	2.02	M2.5 (WMR)	M0-M5	M2.5	Poss. dwarf
6	17			16 27 20.4	−23 58 42	...	> −0.2	17.40	1.34	U (WMR)	M0-M3	M1	
6	21			16 27 25.2	−23 55 54	...	1.0	13.41	1.34	...	K2-K3	K2	
2	40			16 27 28.9	−24 09 38	...	2.8	14.85	1.48	...	F2-F4	F3.5	
3	38	Same as 2-40				...	2.9				F2-F5		
1	13	ISO-Oph 149	ROXRF 26	16 27 30.9	−24 47 26	...	−7.2	16.17	2.15	...	M1-M2	M1	
6	44	UCAC3		16 27 31.3	−23 59 09	...	0.30	13.12	1.02	M1 (WMR)	M0-M1	M1	Poss. dwarf
1	17	ISO-Oph 155/GY 292	[IKT2001] 69	16 27 33.2	−24 41 14	...	−60	15.65	2.01	K8 (LR)	K5-K6	K6	
5	59	Same as 1-17				...	−80				K6-M0		

Table 2  
(Continued)

<i>F</i>	Ap. <sup>a</sup>	Name(s) <sup>b</sup>	X-Ray ID <sup>c</sup>	R.A.(J2000) (hhmmss.s)	Decl.(J2000) (° ' ")	Li?	EW(H $\alpha$ )	<i>I</i>	( <i>R</i> − <i>I</i> ) <sup>d</sup> (mag)	Prev Sp. Ty. <sup>e</sup> (mag)	Sp. Ty.	Adopt	Notes
1	7	GY 297		16 27 36.5	−24 28 33	...	<0.2	13.32	1.35	M2 (WMR)	M2-M3.5	M3	
2	46	Same as 1-7				...	<0.2				M2-M3		
5	88	Same as 1-7				...	0.30				M3-M4		
6	18	Same as 1-7				...	0.40				M2-M3		
2	7			16 27 36.9	−23 58 27	Yes:	−10	16.02	2.15	...	M4-M5.5	M4.5	
1	9	WLY 2-48/ISO-Oph 159		16 27 37.3	−24 30 34	...	10+em	14.67	1.99	M0 (G)	B5-F2	A0	
2	35			16 27 38.0	−23 57 24	Yes	−2.8	13.73	1.72	M2.5 (WMR)	M1-M3	M2.5	
2	31	UCAC3	ROXC J162738.2-240401	16 27 38.5	−24 04 02	Yes	−1.4	13.41	1.58	...	K5-K6	K5.5	
1	31			16 27 43.6	−24 51 25	...	1.0	14.26	1.51	...	K1-K2	K2	
1	14			16 27 45.2	−25 03 33	Yes	−5.7	14.07	1.85	M4.5 (WMR)	M3-M5	M3.5	
6	79			16 27 49.3	−23 56 09	...	<0.8	16.50	1.04	G2.5 (WMR)	F6-K0	G2.5	
5	28	UCAC3		16 27 54.4	−24 51 60	...	0.70	13.63	1.27	...	K3-K5	K4	
6	23			16 27 59.7	−23 57 16	...	> −0.4	17.01	1.74	M0 (WMR)	K8-M0	M0	
2	30			16 28 00.8	−24 00 52	Yes	−3.8	13.90	1.84	M3 (WMR)	M2	M2	
2	27			16 28 01.4	−24 02 11	...	1.1	14.62	1.48	...	G5-K0	G9	
2	4			16 28 02.2	−24 19 05	...	3.3	15.31	1.66	...	F1-F3.5	F2	
1	11			16 28 03.4	−24 53 22	Yes	−9.2	14.41	2.11	...	M5-M6	M5.5	
6	78			16 28 04.9	−23 56 08	...	1.1	17.28	1.22	K5 (WMR)	G5-K2	G9	
2	21			16 28 05.9	−24 29 12	...	0.90	15.48	1.79	...	K0-K2	K1	
2	12			16 28 06.6	−24 18 55	...	2.4	14.79	1.48	...	F7-G4	G0	
2	43	UCAC3		16 28 08.1	−24 04 49	...	0.80	13.36	1.58	...	K1-K4	K3	
5	41			16 28 09.9	−24 48 48	...	> −0.4	16.68	0.86	K4.5 (WMR)	K0-K5	K4.5	
5	98			16 28 11.0	−24 55 57	...	> −0.4	15.92	2.00	...	K0-K5	K3:	
2	18			16 28 11.1	−24 06 18	Yes	−6.3	14.29	2.10	M3.75 (WMR)	M3-M4.5	M3.75	
2	22			16 28 11.2	−24 29 19	...	0.80	15.44	1.70	...	G9-K0	G9	
2	62			16 28 12.3	−24 09 28	...	0.90	13.37	2.26	...	M2.5-M4	M3.5III	Giant
5	17	Same as 2-62				...	1.2				M2.5-M4.5		
6	34	Same as 2-62				...	1.2				M3-M4		
1	24	ISO-Oph 194	ROXC J162813.7-243249	16 28 13.9	−24 32 49	...	−11	15.72	2.36	...	M3-M4.5	M4	
5	73			16 28 13.9	−24 56 10	Yes	−3.5	14.13	1.45	...	K7-M0	M0	
6	27			16 28 14.4	−23 57 52	...	> −1.4	17.53	1.12	G7 (WMR)	G0-K5	G7	
2	26	AOC 7		16 28 14.9	−24 23 22	...	−2.3	15.32	1.71	...	G9-K2	K0:	
2	39			16 28 15.8	−24 09 32	...	1.1	15.73	1.78	...	G9-K2	K0	
5	94			16 28 16.6	−24 07 36	...	> −2.0	16.79	1.67	U (WMR)	U	M0	
6	7	Same as 5-94				...	<0.3				K6-M1		
2	10	ISO-Oph 195	RXJ 1628.2-2405	16 28 16.9	−24 05 15	Yes	< −3.4	13.91	1.68	K5 (MMGC)	K5-K6	K6	
1	32			16 28 17.6	−24 33 54	...	1.0	15.30	1.97	...	K3-K5	K3	
5	91	Same as 1-32				...	<0.1				U		
6	49	Same as 1-32				...	<1.0				G9-K3		
2	53			16 28 18.8	−24 20 15	...	<0.2	15.01	2.00	...	M0-M5	M1III	Giant

Table 2  
(Continued)

<i>F</i>	Ap. <sup>a</sup>	Name(s) <sup>b</sup>	X-Ray ID <sup>c</sup>	R.A.(J2000) (hhmmss.s)	Decl.(J2000) (° ′ ″)	Li?	EW(H $\alpha$ )	<i>I</i>	( <i>R</i> − <i>I</i> ) <sup>d</sup> (mag)	Prev Sp. Ty. <sup>e</sup> (mag)	Sp. Ty.	Adopt	Notes
5	62	Same as 2-53				...	0.90				K7-M2		
5	29			16 28 20.0	−24 26 11	...	> −0.2	15.70	1.20	G5 (WMR)	U	G5	
2	59			16 28 20.1	−24 23 18	...	−4.2	15.65	2.04	M3.5 (WMR)	M3-M4	M3.5	
5	16			16 28 21.5	−24 48 15	...	0.70	15.09	1.55	...	K5-K6	K5	
2	6		ROXC J162821.5-242155	16 28 21.6	−24 21 55	Yes	−3.3	14.99	1.98	M2.5 (WMR)	M2-M3	M2.5	
2	41			16 28 21.7	−24 17 45	...	1.5	15.29	1.65	...	F9-G4	G1	
1	10			16 28 23.0	−24 48 28	...	−14	15.74	2.10	...	M3.5-M5	M5	
2	9			16 28 24.8	−24 08 14	...	1.2	16.53	1.54	...	K4-K6	K4:	
6	33	Same as 2-9				...	> −0.1				K3-K5		
1	26			16 28 24.9	−24 35 43	Yes:	−9.0	14.80	1.98	M5 (WMR)	M3.5-M5	M5	
5	12			16 28 28.3	−24 52 22	...	0.50	15.03	1.37	K6 (WMR)	K5-K6	K6	
5	21			16 28 28.3	−23 58 51	...	<2.0	17.04	1.31	U (WMR)	U	U	
5	49			16 28 29.4	−24 31 21	...	<0.1	16.57	1.20	K0 (WMR)	G9-K5	K0	
6	37	Same as 5-49				...	0.50				K3-K5		
2	37			16 28 31.2	−24 02 34	...	0.6	14.41	1.93	...	K4-K6	K5:	
2	44			16 28 32.4	−24 05 49	...	−6.4	15.44	2.35	...	M3-M4	M3.5	
2	45			16 28 32.6	−24 15 24	...	−11	15.97	2.33	M3.5 (WMR)	M3-M4	M3.5	
5	84			16 28 36.3	−24 00 43	...	<1.0	16.31	1.53	K1 (WMR)	G5-K6	G5:	
6	56	Same as 5-84				...	1.6				F6-K0		
2	16		ROXC J162843.1-242251	16 28 43.1	−24 22 52	Yes:	−6.8	14.47	2.07	M4.75 (WMR)	M3-M5	M4	
5	51			16 28 43.5	−24 52 18	...	1.3	12.97	1.08	...	K0-K4	K2	
5	44			16 28 43.6	−24 04 44	...	1.7	15.77	1.25	G0 (WMR)	F6-K0	G0	
2	47			16 28 43.9	−24 06 41	...	0.9	14.32	1.80	...	K6-M0	M0III	Giant
5	7	AOC 27		16 28 47.2	−24 28 13	...	−190	16.00	2.05	...	M3.5-M5.5	M4.5	
5	74			16 28 48.6	−24 04 41	...	<0.6	14.74	1.41	...	F0-G9	G0:	
6	50	Same as 5-74				...	1.9:				F6-G9		
2	54			16 28 49.8	−23 55 08	...	> −0.5	15.17	1.65	...	M3-M4	M3.5	
6	25	Same as 2-54				...	> −0.2				M3-M4		
2	25			16 28 51.6	−24 06 11	...	1.9	15.37	1.31	...	G2-G4	G3	
5	97	UCAC3		16 28 52.1	−24 47 39	...	0.80	13.62	1.70	...	K3-K5	K2	
5	20	AOC 73		16 28 56.9	−24 38 10	...	1.0	15.44	1.65	...	K3-K6	K3:	
5	4	AOC 40	ROXC J162856.8-243109	16 28 57.1	−24 31 09	...	−52	15.39	2.08	...	M5-M6	M5.5	
2	50	WSB 65		16 28 58.9	−24 04 23	...	1.5	14.52	1.44	...	G3-G5	G4	
5	93			16 28 59.2	−24 05 16	...	> −0.4	17.05	1.69	G2.5 (WMR)	F1-K5	G2.5	
6	9	Same as 5-93				...	> −1.0				U		
6	4			16 29 00.0	−24 26 39	...	<1.0	15.24	0.96	G9 (WMR)	U	G9	
2	36			16 29 02.0	−23 56 23	...	<0.4	14.46	2.00	...	M3-M3.5	M3.5III	Giant
5	53			16 29 02.0	−24 31 11	...	> −0.2	17.43	0.89	G7.5 (WMR)	G9-K6	K0	
2	57			16 29 03.1	−24 27 49	...	−12	13.19	1.95	...	M3.5-M5.5	M5	
6	31	Same as 2-57				Yes	−17				M3-M5		

**Table 2**  
(Continued)

<i>F</i>	Ap. <sup>a</sup>	Name(s) <sup>b</sup>	X-Ray ID <sup>c</sup>	R.A.(J2000) (hhmmss.s)	Decl.(J2000) (° ' ")	Li?	EW(H $\alpha$ )	<i>I</i>	( <i>R</i> − <i>I</i> ) <sup>d</sup> (mag)	Prev Sp. Ty. <sup>e</sup> (mag)	Sp. Ty.	Adopt	Notes
5	96			16 29 03.7	−24 30 02	...	<0.5	16.55	1.70	...	M2-M4	M3	
6	6	UCAC3		16 29 06.9	−23 55 16	...	1.6	13.97	1.44	...	K1-K3	K2	
5	25			16 29 11.6	−24 22 15	...	> − 0.1	17.79	1.09	G0.5 (WMR)	F0-K5	G0.5	
6	77	Same as 5-25				...	> − 1.0				K0-K6		
2	42			16 29 14.3	−24 25 42	...	2.2	15.96	0.82	...	F9-G3	G1	
2	19			16 29 14.4	−24 11 53	...	0.80	15.68	1.90	...	K3-K4	K4	
5	87			16 29 20.1	−24 21 32	...	−7.0	17.67	1.01	U (WMR)	K6-M2	M0	
5	71	UCAC3		16 29 21.7	−24 45 09	...	0.80	13.23	1.35	...	K3	K3	
5	33			16 29 23.5	−24 27 51	...	> − 0.8	17.52	0.83	K1 (WMR)	U	K1	
5	35			16 29 23.8	−24 43 54	...	0.90	14.03	1.33	...	K0-K4	K1	
5	34	UCAC3		16 29 23.9	−24 29 11	...	<0.2	16.15	0.97	G5 (WMR)	U	G5	
5	24			16 29 24.5	−24 30 55	...	> − 0.3	17.66	0.87	G2.5 (WMR)	G0-M0	G2.5	
2	8			16 29 24.6	−24 09 01	...	0.90	14.36	1.43	...	G8-K0	G9	
2	33	UCAC3		16 29 24.8	−24 06 48	...	1.0	14.12	1.45	...	K0-K2	K1	
5	31			16 29 25.6	−24 39 35	...	1.0	13.97	1.78	...	K1-K5	K3	
2	14			16 29 27.2	−24 23 18	...	<0.2	16.00	1.49	...	M2-M3	M3	
2	17			16 29 28.7	−24 21 26	...	2.1	15.85	0.83	...	F7-G4	G0	
2	49			16 29 32.2	−24 05 49	...	0.80	14.30	1.40	...	K1-K3	K3	
5	77			16 29 32.5	−24 36 06	...	<0.2	14.78	1.63	...	K4-K5	K5	

**Notes.**

<sup>a</sup> HYDRA field and aperture number of observation.

<sup>b</sup> Sources names from optical or infrared studies by (GSS, Source 2) Grasdalen et al. 1973; (VSSG) Vrba et al. 1975; (VSS) Vrba et al. 1976; (WSB) Wilking et al. 1987; (WLY) Wilking et al. 1989; (GY) Greene & Young 1992; (ISO-Oph) Bontemps et al. 2001; (AOC) Alves de Oliveira & Casali 2008; and (UCAC3) Zacharias et al. 2009.

<sup>c</sup> X-ray source association from the EINSTEIN survey by (ROX) Montmerle et al. 1983, the ROSAT surveys by (RXJ) Martín et al. 1998 and (ROXRF) Grosso et al. 2000, the Chandra surveys by ([IKT2001]) Imanishi et al. 2001 and (ROXC) N. Grosso 2005, private communication, or the XMM-Newton survey by (ROXN) Ozawa et al. 2005.

<sup>d</sup> *R*- and *I*-band photometry from this study except for ROX 3 which are from S. Gordon & K. M. Strom 1990, unpublished data.

<sup>e</sup> References for spectral types: (BA) Bouvier & Appenzeller 1992; (MMGC) Martín et al. 1998; (LR) Luhman & Rieke 1999; (WMR) Wilking et al. 2005; (G) Geers et al. 2007.

**Table 3**  
Association Members with Optical Spectra

F	Ap.	Name(s) <sup>a</sup>	WMR <sup>b</sup>	Sp. Type <sup>c</sup>	$A_v$ <sup>d</sup> (mag)	$M(I)$ (mag)	$\log T_{\text{eff}}$ (K)	$\log(L/L_{\odot})$	$M_*$ <sup>e</sup> ( $M_{\odot}$ )	$\log(\text{age})$ (yr)	Criteria <sup>f</sup>	Notes <sup>g</sup>
4	40			M4.5	2.1	9.03	3.488	-1.79	0.15	7.18	ext	
4	29			M2	5.6	6.23	3.544	-0.82	0.32	6.46	ext	
3	37			K7	6.8	3.96	3.602	0.06	0.42	5.65	ext	
4	42			M4.5	2.3	7.83	3.488	-1.31	0.16	6.57	ext	
		RXJ 1624.9-2459		K5 (MMGC)	0.3 (2M)	6.91	3.638	-1.44	...	...	pm,x	(1)
3	58		2-15	M3.5	2.6	6.60	3.512	-0.90	0.19	6.23	ext,li	
4	59	WSB 18		M3.5	2.7	6.58	3.512	-0.89	0.19	6.23	ext,ha,IRX	(4)
4	82	WSB 19		M4.5	0.2	7.46	3.488	-1.16	0.16	6.38	ha,IRX	
4	38			M5	1.8	9.13	3.477	-1.78	0.12	7.01	ext,ha	
4	32			K6	7.0	5.03	3.621	-0.40	0.73	6.61	ext	
4	52			M3	5.0	6.40	3.525	-0.85	0.23	6.27	ext,ha	
		GSS 5		G9 (TQ)	0.6 (GS)	3.08	3.729	0.47	1.7	6.65	pm,x	(4)
		SR 22	2-10	M5	0.7	8.51	3.477	-1.53	0.14	6.75	ha	
		HD 147889	1-7	M4.5	0.0 (GS)	7.31	3.488	-1.10	0.16	6.31	ha,pm,x	
				B2 (HS)	4.4 (C)	-1.76	4.320	3.63	8.3	zams?	pm,ref. neb.	(2)
3	45			K7	6.7	4.89	3.602	-0.32	0.55	6.24	ext	
		ROXR1-4/SR 8		K7 (MMGC)	1.6 (2M)	3.81	3.602	-0.18	0.49	5.98	ext,pm,x	
4	17			M0	4.3	7.49	3.580	-1.34	0.52	7.98	ext	
3	5			K6:	7.8	4.92	3.621	-0.35	0.70	6.51	ext	
3	56	WLY 2-2		K4	6.7	3.79	3.662	0.12	0.80	6.08	ext,IRX,li	(4)
		WLY 2-3	3-15	M2	4.8	6.42	3.544	-0.90	0.32	6.58	ext,ha,IRX,x	
			2-32	M3.5	2.5	7.20	3.512	-1.14	0.21	6.54	ext,li,x	
4	16	ROX 3		K8	1.1 (GS)	4.82	3.591	-0.28	0.47	6.06	li,pm,x	
		VSS 23	1-22	K5.5	5.0	3.81	3.630	0.10	0.56	5.78	ext,pm,x	
1	3			K0	6.6	3.96	3.720	0.11	1.3	6.95	ext,pm	
		WLY 2-11	2-25	M5	2.1	7.71	3.477	-1.22	0.14	6.39	ext,ha,x	
		SR 4	1-29	K4.5	2.8 (BA)	3.45	3.650	0.25	0.66	5.75	ext,ha,IRX,li,pm,x	
		GSS 20	1-38	K5.5	5.9	3.92	3.630	0.05	0.57	5.85	ext,pm,x	
1	16		3-14	M4	1.8	7.22	3.498	-1.12	0.18	6.40	ext,li	
		Chini 8	2-1	M5.5	0.0	7.47	3.462	-1.06	0.12	6.09	ha,li,x	
			4-28	M3	5.2	6.33	3.525	-0.82	0.23	6.24	ext,x	
		GSS 23		K0 (MMGC)	7.1 (BA)	1.09	3.720	1.26	2.9	5.69	ext,pm,x	
		VSSG 19	1-13	M2	3.3	5.43	3.544	-0.50	0.29	6.00	ext,x	(4)
			2-19	M4.5	1.7	7.21	3.488	-1.06	0.16	6.27	ext,ha,li	
		SR 3		B6 (EL)	6.5 (C)	0.28	4.146	2.28	3.8	6.13	pm	(3)
3	43	GSS 29		K6	9.3	4.06	3.621	0.00	0.54	5.86	ext,IRX,li	
		GSS 28	1-5	K4.5	2.9	4.54	3.650	-0.18	0.85	6.52	ext,ha,IRX,li,pm,x	
3	15		4-39	M3.25	2.3	6.14	3.519	-0.73	0.20	6.09	ext,li	
			2-11	M4.75	0.0	7.75	3.482	-1.25	0.15	6.46	li,x	
		WSB 28	1-25	M2	2.7	5.92	3.544	-0.70	0.36	7.99	ext,ha,pm,x	
		GY 5	4-16	M5.5	2.0	9.15	3.462	-1.74	0.11	5.06	ext,ha,IRX,x	
		GY 3	4-41	M8	0.0	10.1	3.398	-1.45	0.04	5.43	ha,IRX,x	
		GSS 31	1-30	G6	7.6 (GS)	1.41	3.752	1.16	2.8	6.23	ext,IRX,pm,x	
		DoAr 25	1-28	K5	3.6 (GS)	3.65	3.638	0.16	0.60	5.76	ext,ha,IRX,li,pm,x	
		EL 24	2-27	K5.5	7.6	3.86	3.630	0.08	0.57	5.81	ext,ha,IRX,x	
3	23	GSS 32/Source 2		K5	10	3.90	3.638	0.06	0.63	5.92	ext,IRX,x	
3	51		4-18	M4.5	2.1	9.01	3.488	-1.78	0.15	7.17	ext,ha	
			4-25	M5.5	1.1	9.57	3.462	-1.90	0.08	6.87	x	
		WSB 34	2-36	M4.5	0.7	8.16	3.488	-1.44	0.16	6.75	ha	
		Source 1	1-2	B3	13	-0.77	4.301	3.20	6.0	zams?	ext,ref. neb.,x	(3)(4)
3	16	ISO-Oph 51		M0	4.9	7.13	3.580	-1.20	0.57	7.73	ext,IRX,li,x	
			4-4	M5	1.9	8.83	3.477	-1.66	0.13	6.89	ext,ha,x	
		WSB 37	2-29	M5	0.7	7.40	3.477	-1.09	0.14	6.24	ha,IRX,li,x	
3	18	GSS 37/VSSG 2		M1	6.1	5.13	3.562	-0.39	0.36	5.99	ext,ha,IRX,li,x	
3	33		1-21	K8	4.2	5.25	3.591	-0.45	0.56	6.40	ext,li,pm,x	
1	21			K6	4.4	6.09	3.621	-0.82	0.72	7.51	ext	
		GY 112	1-20	M3	2.2	6.34	3.525	-0.82	0.23	6.24	ext,pm,x	
1	22		3-22	M4	1.0	7.74	3.498	-1.33	0.18	6.68	li,x	
3	36		4-13	M3	4.6	7.20	3.525	-1.16	0.25	6.73	ext	
		WSB 38	1-36	G3.5	7.4	2.38	3.765	0.78	1.8	6.78	ext,ha,IRX,li,pm,x	(4)
			4-30	M4.5	2.7	8.04	3.488	-1.40	0.16	6.68	ext,li,var,x	
1	8		4-59	M5	2.0	8.80	3.477	-1.65	0.13	6.88	ext,x	
		WSB 40	1-32	K5.5	5.3	4.20	3.630	-0.06	0.61	6.04	ext,ha,pm	
		WL 18	4-53	K6.5	12 (2M)	4.63	3.612	-0.52	0.74	6.78	ext,ha,IRX,x	
2	56		2-38	M3.5	3.3	7.26	3.512	-1.16	0.21	6.58	ext,li,var	

**Table 3**  
(Continued)

F	Ap.	Name(s) <sup>a</sup>	WMR <sup>b</sup>	Sp. Type <sup>c</sup>	$A_v$ <sup>d</sup> (mag)	$M(I)$ (mag)	$\log T_{\text{eff}}$ (K)	$\log(L/L_{\odot})$	$M_*$ <sup>e</sup> ( $M_{\odot}$ )	$\log(\text{age})$ (yr)	Criteria <sup>f</sup>	Notes <sup>g</sup>
			4-46	K7	8.7	5.54	3.602	-0.57	0.71	6.80	ext,ha,IRX,x	
		SR 24s	1-37	K1	6.2	3.45	3.705	0.30	1.5	6.52	ext,ha,IRX,pm,x	
		SR 24n		M0.5 (CK)	8.9 (2M)	2.32	3.571	0.32	0.47	<6.0	ext,ha,IRX	(3)(4)
2	32			M1	4.1	6.00	3.562	-0.74	0.45	6.61	ext,li,x	
5	67			K8	5.5	6.09	3.591	-0.79	0.71	7.15	ext,li	
1	5	GY 194		M0	6.0	6.47	3.580	-0.93	0.64	7.26	ext,li,x	
		GY 204	4-65	M5.5	0.4	9.63	3.462	-1.93	0.08	6.88	ha,IRX,var,x	
2	29		4-63	M4.5	2.5	8.26	3.488	-1.48	0.16	6.80	ext,ha	
5	81	ISO-Oph 106	4-37	M2.5	6.4	6.74	3.535	-1.01	0.28	6.61	ext,ha,IRX	
		SR 21		G1 (MMGC)	7.6 (GS)	1.12	3.774	1.29	2.9	6.26	ext,IRX,pm,x	
2	23			K6	7.7	5.16	3.621	-0.46	0.77	6.72	ext,li,x	
		WSB 45	3-44	M4.5	0.0	7.75	3.488	-1.29	0.16	6.52	li,pm,x	
		WSB 46	1-9	M2	0.5	6.41	3.544	-0.89	0.32	6.57	pm,x	
			4-10	M3.5	4.3	7.37	3.512	-1.20	0.21	6.65	ext,ha,x	
6	62			K8	4.9	4.72	3.591	-0.24	0.46	5.99	ext	
		WSB 48	1-6	M3.75	0.0	7.66	3.491	-1.31	0.17	6.59	ha,pm	
		SR 12		M0	2.3 (GS)	4.00	3.580	0.05	0.33	5.46	ext,pm,x	(4)
		WSB 49	3-6	M4.25	0.3	7.53	3.493	-1.22	0.17	6.49	ha,IRX,li,pm,x	
		GY 264	4-45	M8	0.0	10.2	3.398	-1.50	0.04	5.47	ha,var,x	
			3-7	M4.75	0.0	8.75	3.482	-1.65	0.14	6.95	x	
		GY 280	2-20	M2	1.0	8.16	3.544	-1.59	0.36	7.73	x	(5)
		GY 284	4-22	M3.25	4.9	7.75	3.519	-1.37	0.24	6.98	ext,IRX,x	
		GY 292		K5 (LR,GS)	8.9	4.77	3.638	-0.28	0.80	6.58	ext,IRX,x	
		WSB 50	2-6	M4.5	1.9	7.36	3.488	-1.12	0.16	6.33	ext,li,x	
2	7			M4.5	2.3	9.04	3.488	-1.80	0.15	7.19	ext,ha,li:	
		ROX 30A		K3 (GS)	4.1	5.19	3.676	-0.42	0.90	7.25	ext,x	
1	9	WLY 2-48/ISO-Oph 159		A0	12	1.68	3.979	1.31	2.1	7.53	ext,IRX	
2	35		4-54	M2.5	2.9	6.44	3.535	-0.89	0.27	6.43	ext,li	
		WLY 2-49	4-24	K5.5	9.6	4.16	3.630	-0.04	0.61	6.01	ext,ha,IRX,x	
		WSB 51	2-35	K6	4.1	4.29	3.621	-0.10	0.57	6.01	ext,ha,li,pm,x	
2	31			K5.5	5.9	4.29	3.630	-0.09	0.63	6.10	ext,li,x	
		WSB 53	1-31	K5.5	3.4	4.43	3.630	-0.15	0.66	6.21	ext,ha,pm	
		WSB 52	3-5	K5	7.0	4.26	3.638	-0.08	0.69	6.18	ext,ha,IRX,li,x	
		SR 9	1-26	K5	1.3 (BA)	3.57	3.638	0.20	0.59	5.71	ha,IRX,li,pm,x	(4)
			2-34	M2	3.9	5.52	3.544	-0.54	0.29	6.04	ext,x	
		GY 326	4-64	M2	9.6 (2M)	5.01	3.544	-0.77	0.31	6.38	ext,IRX,x	
1	14		3-21	M3.5	2.2	7.20	3.512	-1.14	0.21	6.54	ext,li	
		VSSG 14	1-14	A7	9.1	1.48	3.895	1.24	2.1	6.76	ext,pm,x	
		ROX 31	1-10	K7.5	5.0	4.12	3.597	0.00	0.41	5.68	ext,x	(4)
		SR 10	1-24	M2	0.0	6.36	3.544	-0.87	0.32	6.54	ha,IRX,pm,x	(4)
		WSB 58	3-34	M4.75	0.7	7.41	3.482	-1.12	0.15	6.31	x	
			3-31	M5	0.8	7.47	3.477	-1.12	0.14	6.28	ha,li,x	
2	30		2-3	M2	4.2	5.79	3.544	-0.65	0.30	6.20	ext,li	
1	11			M5.5	0.3	8.66	3.462	-1.54	0.10	6.59	li	
2	18		2-21	M3.75	3.4	6.70	3.491	-0.92	0.16	6.14	ext,li	
		ROX 32	3-11	M3	3.4	6.08	3.525	-0.72	0.22	6.12	ext,li,x	
5	73			M0	3.4	6.55	3.580	-0.97	0.63	7.33	ext,li	
1	24	ISO-Oph 194		M4	4.6	7.41	3.498	-1.19	0.18	6.50	ext,ha,IRX,x	
		WSB 60	3-20	M4.5	1.9	7.73	3.488	-1.27	0.16	6.51	ext,ha,IRX	
2	10	ISO-Oph 195		K6	6.3	4.57	3.621	-0.21	0.63	6.23	ext,IRX,li,x	
			3-12	M3	1.9	6.80	3.525	-1.01	0.24	6.49	ext	
2	59		4-3	M3.5	3.4	8.05	3.512	-1.48	0.22	7.07	ext	
2	6		2-37	M2.5	4.5	6.72	3.535	-1.00	0.28	6.61	ext,IRX,li,x	
1	10			M5	1.2	9.45	3.477	-1.91	0.11	7.13	ha	
			2-30	K5	6.7	5.03	3.638	-0.39	0.86	6.80	ext,ha,IRX,x	
			2-4	M2	4.6	6.26	3.544	-0.83	0.32	6.48	ext,x	
1	26		3-39	M5	0.4	8.98	3.477	-1.72	0.13	6.95	li	
		HD 148352		F2 (HS)	0.0 (2M)	1.18	3.838	1.21	2.1	6.71	x	(5)
2	44			M3.5	5.3	6.68	3.512	-0.93	0.20	6.27	ext	
2	45		4-57	M3.5	5.2	7.28	3.512	-1.17	0.21	6.59	ext,ha	
		SR 20	1-35	G7	7.0 (GS)	1.46	3.747	1.14	2.8	6.22	ext,ha,pm,x	(4)
2	16		2-23	M4	2.8	7.25	3.498	-1.13	0.18	6.41	ext,li,x	
		SR 13	1-15	M3.75	0.0 (BA)	5.33	3.491	-0.38	0.14	4.77	ha,IRX,pm,x	(4)
5	7			M4.5	1.8	9.36	3.488	-1.93	0.14	7.34	ext,ha,var	
		WSB 63	3-43	M1.5	3.9	5.61	3.553	-0.58	0.35	6.20	ext,ha,li,x	

**Table 3**  
(Continued)

F	Ap.	Name(s) <sup>a</sup>	WMR <sup>b</sup>	Sp. Type <sup>c</sup>	$A_v$ <sup>d</sup> (mag)	$M(I)$ (mag)	$\log T_{\text{eff}}$ (K)	$\log(L/L_{\odot})$	$M_{*}$ <sup>e</sup> ( $M_{\odot}$ )	$\log(\text{age})$ (yr)	Criteria <sup>f</sup>	Notes <sup>g</sup>
5	4			M5.5	0.2	9.73	3.462	-1.97	0.08	6.91	ha,IRX,var,x	
2	57			M5	0.3	7.46	3.477	-1.12	0.14	6.28	ha,IRX,li	
			3-37	M5.5	0.0	8.91	3.462	-1.64	0.10	6.67	li	
		ROX 35A		K3 (BA)	2.1 (W)	3.93	3.676	0.08	1.0	6.36	ext,li,x	
		ROX 35B		G4 (BA)	2.5 (GS)	3.64	3.763	0.27	1.2	7.22	ext,x	

**Notes.**

<sup>a</sup> Sources names from optical or infrared studies noted in Table 2 plus: (SR) Struve & Rudkjøbing 1949; (DoAr) Dolidze & Arakelyan 1959; (EL) Elias 1978; (Chini) Chini 1981; (WL) Wilking & Lada 1983; and (ROXR1) Casanova et al. 1995.

<sup>b</sup> Source name from Wilking et al. (2005).

<sup>c</sup> Optical spectral types from this study or Wilking et al. (2005) except where noted: (EL) Elias 1978; (CK) Cohen & Kuhl 1979; (HS) Houk & Smith-Moore 1988; (GS) S. Gordon & K. M. Strom 1990, private communication; (BA) Bouvier & Appenzeller 1992; (TQ) Torres et al. 2006; and (MMGC) Martín et al. 1998.

<sup>d</sup>  $R$ - and  $I$ -band magnitudes used to compute  $A_v$  and  $L_{\text{bol}}$  are from this study except where noted: (C) Chini 1981; (GS) S. Gordon & K. M. Strom 1990, private communication; (BA) Bouvier & Appenzeller 1992; and (W) Walter et al. 1994. (2M) denotes  $J$ - and  $H$ -band data from 2MASS were used to compute  $A_v$  and  $L_{\text{bol}}$  and  $M(J)$  replaces  $M(I)$  in Column 7.

<sup>e</sup> Masses and ages estimated from the tracks and isochrones of D'Antona & Mazzitelli 1997 and F. D'Antona & I. Mazzitelli 1998, private communication except where noted in the last column.

<sup>f</sup> Association membership established through location above the main sequence and  $A_v > 1.5$  mag (ext), the presence of  $H\alpha$  emission  $\text{EW} > 10 \text{ \AA}$  (ha), an infrared excess (IRX), lithium absorption (li), proper motion (pm), reflection nebosity (ref. neb.), near-infrared variability (var), or X-ray emission (x). See the text for details.

<sup>g</sup> Notes: (1) sits below main sequence, possible foreground star; (2) spectroscopic binary Casassus et al. 2008; (3) mass and age derived from the tracks and isochrones of Palla & Stahler 1999; (4) subarcsecond companion observed in infrared and treated as a single object (Barsony et al. 2003; Prato 2007); (5) discordant proper motion (Mamajek 2008).

1989). Star symbols mark the locations of the multiple B star  $\rho$  Oph and the three most massive members of the L 1688 embedded cluster: HD 147889, Source 1, and SR 3. While the association members are concentrated toward the molecular gas, there is marked lack of association members in the direction of the cold, dense cores B and E. A comparison of this distribution with that of association members identified at all wavelengths (Wilking et al. 2008) confirms that we are missing the youngest and most highly obscured YSOs in the cloud.

#### 4.4. Hertzsprung–Russell Diagram

To derive luminosities, we began by dereddening sources using the  $(R-I)$  color index assuming the reddening law derived by Cohen et al. (1981) in the Kron–Cousins system:

$$A_v = 4.76E(R - I), \text{ Sp Ty} < A0 \text{ (early-type)} \quad (1)$$

$$A_v = 6.25E(R - I), \text{ Sp Ty} \geq A0 \text{ (late-type)}, \quad (2)$$

where  $R = 3.2$  for early-type stars and  $3.8$  for late-type stars.  $R$ - and  $I$ -band data were taken from this study except where noted in Column 6 of Table 3. For five sources,  $R$ - and  $I$ -band data were not available and sources were dereddened using  $J$ - and  $H$ -band data from the 2MASS survey (Cutri et al. 2003) and transformed into the CIT photometric system using the relationships derived by Carpenter (2001). A sixth source (WL 18) was dereddened using  $J$  and  $H$  magnitudes since strong  $H\alpha$  emission distorts its  $R$ -band magnitude. In these latter cases, we used the relation for the CIT photometric system

$$A_v = 9.09E(J - H) \text{ (Cohen et al. 1981)}. \quad (3)$$

In a few instances, the errors in the photometry and/or spectral classifications yielded negative values for the extinction of a few tenths and an extinction of 0.0 was assumed.

Effective temperatures were derived from the spectral classifications with typical uncertainties of  $\pm 150$  K for K–M stars. We

note that the assumption of dwarf, rather than subgiant, surface gravities will *overestimate*  $T_{\text{eff}}$  for stars with spectral types of G5–K5 by  $< 250$  K and *underestimate*  $T_{\text{eff}}$  for stars with spectral types of M2–M8 by  $< 200$  K (e.g., Drilling & Landolt 2000). Intrinsic colors and bolometric corrections for dwarf stars were taken from the works of Schmidt–Kaler (1982) for B8–K5 stars and from Bessell (1991) for K5–M7 stars. For the three B stars, we adopted the intrinsic colors, bolometric magnitudes, and temperatures from Drilling & Landolt (2000), converting the colors into the Kron–Cousins system. For the M8 brown dwarf candidates, we assumed values of  $T_{\text{eff}} = 2400$ ,  $(R - I)_0 = 2.5$ , and  $\text{BC}(I) = -1.7$  (Dahn et al. 2002; Hawley et al. 2002).

The absolute  $I$  magnitude,  $M(I)$ , was computed given the extinction and assuming a distance of 130 pc. We then derived the bolometric magnitude and luminosity given

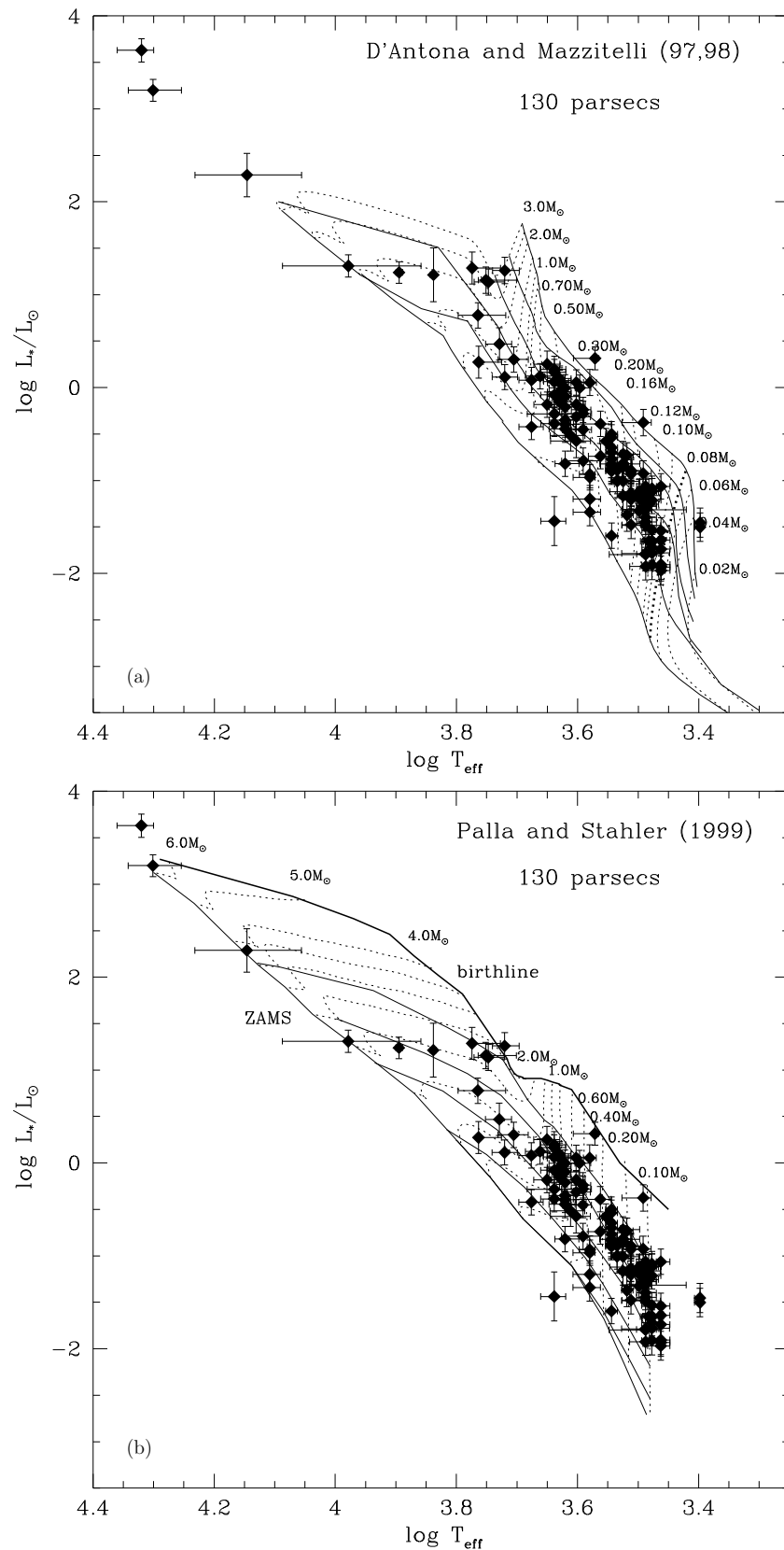
$$M_{\text{bol}} = M(I) + \text{BC}(I), \quad (4)$$

and

$$\log(L_{\text{bol}}/L_{\odot}) = 1.89 - 0.4M_{\text{bol}}, \quad M_{\text{bol}}(\odot) = 4.74. \quad (5)$$

In the situations where  $J$  and  $H$  were used to deredden,  $M(J)$  is recorded in Column 7 of Table 3 and was used along with  $\text{BC}(J)$  to derive  $M_{\text{bol}}$ . The median error in  $\log(L)$  is computed to be 0.14 dex by adding quadratically errors in the  $R$  and  $I$  photometry, an uncertainty in the distance modulus of 0.17 mag corresponding to a depth of 10 pc, and an uncertainty 0.03 mag in the intrinsic color and 0.1 mag in the bolometric correction due to spectral type errors. In most cases the dominant error was the uncertainty in the distance modulus.

H–R diagrams for 135 association members were made using tracks and isochrones from D'Antona & Mazzitelli (1997, DM), F. D'Antona & I. Mazzitelli (1998, private communication), Palla & Stahler (1999, PS99), and Siess et al. (2000). Despite the differences in treatments of the equation of states as a function of mass and of convection, the models give very similar results for our sample. The diagrams for the former two are shown in



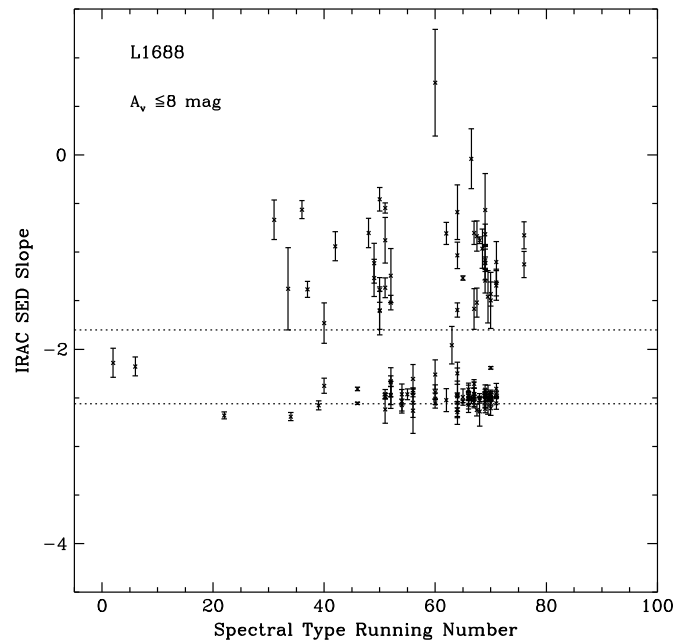
**Figure 4.** Hertzsprung–Russell diagrams for the  $\rho$  Oph association members with optically determined spectral types assuming a distance of 130 pc. The solid diamonds mark the positions of YSOs relative to the theoretical tracks and isochrones of D'Antona & Mazzitelli (1997) and F. D'Antona & I. Mazzitelli (1998, private communication) in (a) or Palla & Stahler (1999) in (b). Error bars in  $\log T_{\text{eff}}$  were estimated from uncertainties in the spectral type and surface gravity. Error bars in  $\log L_{\text{bol}}$  were estimated from errors in the photometry and uncertainties in the distance modulus and bolometric correction. In (a), isochrones shown as solid lines are  $10^5$ ,  $3 \times 10^5$ ,  $10^6$ ,  $3 \times 10^6$ ,  $10^7$ , and  $10^8$  yr. Evolutionary tracks from  $0.02 M_\odot$  to  $2.0 M_\odot$  are shown by dashed lines. The bold dashed line marks the evolutionary track for a star at the hydrogen-burning limit. In (b), the birthline is shown as a solid line followed by isochrones for  $10^6$ ,  $3 \times 10^6$ ,  $10^7$ , and  $10^8$  yr and the ZAMS. Evolutionary tracks from  $0.1 M_\odot$  to  $6.0 M_\odot$  are shown by dashed lines.

Figure 4 as they represent the broadest range in mass. The masses and ages interpolated from the DM models are given in Table 3. Since most of the objects lie on convective tracks, uncertainties in the mass *relative to the DM models* were estimated from the errors in the spectral classifications and uncertainties in the age from errors in the luminosities. Uncertainties in the mass for objects in the range of  $0.08\text{--}1.3 M_{\odot}$  were typically 16%–30%, with the higher value corresponding to the lower mass objects. Uncertainties in the  $\log(\text{age})$  were 0.17–0.25 dex relative to DM models with the greater uncertainty for the higher mass objects. We note that uncertainties in the absolute masses and ages will be larger with theoretical mass tracks underpredicting absolute stellar mass by 30%–50% (Hillenbrand 2009). No age or mass estimate was possible for RXJ 1624.9-2459 as it fell below the  $10^8$  yr isochrone.

#### 4.5. Age Distribution

The values for  $\log(\text{age})$  derived from the DM models are consistent with a normal distribution with an average  $\log(\text{age})$  of  $6.49 \pm 0.05$  (3.1 Myr). Ages derived from the PS99 models agree surprisingly well while the Siess et al. models yield systematically older ages for  $\log(\text{age}) \leq 7.0$ ; the difference can be as much as 0.4 dex for a DM age of 1 Myr. Given the large areal coverage of our survey ( $1.3 \text{ deg}^2$  or  $6.8 \text{ pc}^2$ ), which must include members of the Upper Sco subgroup, an age spread in our sample would not be unexpected. However, simulations do not suggest an *intrinsic* age spread. Assuming Gaussian-distributed errors in  $\log T$  and  $\log L$  and using the DM models for 3 Myr, a Monte Carlo simulation derived values of  $\log T$  and  $\log L$  for over 12,000 samples in the mass range of  $0.12\text{--}1.0 M_{\odot}$  weighted by the Chabrier (2003) system mass function. While the simulated age distribution appears somewhat narrower than what we observe, a Kolmogorov–Smirnov (K-S) test cannot reject the null hypothesis that the two samples are drawn from the same parent population at the 3% level. Lack of strong evidence for a large age spread is consistent with what is found in other young clusters or associations (e.g., Hillenbrand 2009; Slesnick et al. 2008) and supports the idea of rapid star formation (Hartmann 2001).

The average age for this sample is somewhat older than the average of 0.3 Myr derived from more obscured sources in the core using the DM models and dereddened using *JHK* photometry (e.g., Greene & Meyer 1995; Luhman & Rieke 1999; WGM99; Natta et al. 2002). However, we note that there are systematic differences in our derived luminosities, and hence ages, when  $(J-H)$  photometry is used to deredden sources instead of  $(R-I)$ . Using  $(J-H)$  colors from 2MASS yields systematically higher values for  $A_v$  and hence  $L_{\text{bol}}$ . As a consequence, the average  $\log(\text{age})$  for our sample dereddened with  $(J-H)$  colors is  $6.14 \pm 0.05$  (1.4 Myr) compared to  $6.49 \pm 0.05$  (3.1 Myr) when  $(R-I)$  is used. Indeed, a K-S test applied to both versions of our age distributions suggests that the difference is significant. The reason for this discrepancy is not understood but could involve the adopted reddening law (Cohen et al. 1981), surface gravity effects, or possible excess emission in the *J* and *H* bands from optically thick disks. *J*- and *H*-band excesses will overestimate the luminosity which leads to an underestimate of ages (Cieza et al. 2005). Regardless, the older average age for our sample relative to the more obscured sources is significant when both samples are dereddened using  $(J-H)$  (1.3 Myr versus 0.3 Myr) even considering that the previous studies used the pre-*Hipparcos* distance of 160 pc.



**Figure 5.** Spectral indices using the IRAC flux densities as a function of spectral type. The spectral index was computed using a linear least-squares fit to the  $3.6\text{--}8.0 \mu\text{m}$  flux densities. Error bars were calculated from the fit given the statistical uncertainties in the flux densities.

#### 4.6. An Extinction-limited Sample

To explore the frequency of circumstellar disks and the IMF, we considered 123 objects that formed an extinction-limited sample with  $A_v \leq 8 \text{ mag}$ . This sample is representative for objects with  $M \geq 0.2 M_{\odot}$  for an age of 3 Myr using the DM models.

##### 4.6.1. Disk Frequency

Using published data from the *ISO* (Bontemps et al. 2001) and the *Spitzer Space Telescope* (Evans et al. 2009), we can look for a mid-infrared excess relative to the photosphere using the spectral index from  $2.2$  to  $14 \mu\text{m}$  or  $3.6$  to  $24 \mu\text{m}$ , respectively. The spectral index is defined as

$$\alpha = d \log \lambda F_{\lambda} / d \log \lambda.$$

A mid-infrared excess is defined as  $\alpha \geq -1.60$  which is characteristic of an optically thick disk (e.g., Greene et al. 1994). This results in 33 of the 123 sources, or  $27\% \pm 5\%$ , showing evidence for a circumstellar disk lacking a large inner hole (see Table 3) with the uncertainty estimated assuming Poisson statistics (Gehrels 1986). We adopt this disk frequency estimated over near- to mid-infrared wavelengths as the most reliable disk indicator. The sample size is not sufficient for investigating possible variations in the disk frequency with spectral type.

As a check, we can use the slope of the  $3.6\text{--}8.0 \mu\text{m}$  flux densities from the *Spitzer Space Telescope* to assess the fraction of sources with mid-infrared excesses. A linear least-squares fit was made to the flux densities for each source compiled from the *Spitzer* c2d catalog available in NASA/IPAC Infrared Science Archive. Following Lada et al. (2006), disk models suggest that  $\alpha \geq -1.80$  over this wavelength range is indicative of an optically thick disk. The distribution of spectral indices as a function of spectral type is shown in Figure 5. For the 122 sources for which data were available, 40 or  $33\% \pm 5\%$  showed evidence for an optically thick disk consistent with our previous

estimate. We can compare this disk frequency to that derived by Lada et al. for the IC 348 cluster who considered 299 YSOs, most of which reside in an area completely sampled for  $M > 0.3 M_{\odot}$  and  $A_v < 4$  mag (Luhman et al. 2003). Their value of  $30\% \pm 4\%$  for IC 348 is consistent with our disk frequency which is not surprising given the similarity in the cluster’s estimated age of 2–3 Myr (Herbst 2008).

With knowledge of the spectral types, we can also look for evidence of even smaller infrared excesses from the inner disk in the  $K$  band. Using data from the 2MASS survey, we transformed the magnitudes into the CIT system and dereddened them using Equation (3). Assuming that the excess at  $J$  was zero, the difference of the dereddened ( $J-H$ ) color to the intrinsic color was then used to estimate

$$r_H = F_{H_{ex}}/F_H,$$

where  $F_{H_{ex}}$  is the broadband flux from circumstellar emission and  $F_H$  is the expected stellar flux at  $1.6 \mu\text{m}$ . This was then used to estimate the excess at  $K$ :

$$r_K = F_{K_{ex}}/F_K = (1 + r_H) \left( 10^{[(H-K)-(H-K)_0 - 0.065A_v]/2.5} - 1 \right).$$

Values of  $\Delta K = \log(1 + r_K)$  were computed and those that equaled or exceeded 0.20 were associated with an optically thick inner disk (Skrutskie et al. 1990). We note that three sources with an apparent  $K$ -band excess did not display a mid-infrared excess; all three have values close to  $\Delta K = 0.20$  and may be identified as excess sources due to photometric errors. Twenty-three of 123 sources, or  $19\% \pm 4\%$ , showed evidence for an optically thick inner disk. While the assumption of no excess emission at  $J$  could underestimate  $\Delta K$ , the higher percentage of mid-infrared excess sources is typical of young clusters and likely reflects the greater sensitivity of mid-infrared photometry to disk emission (e.g., Meyer et al. 1997; Haisch et al. 2000). The dispersal of the inner disk by accretion, stellar winds, and/or planet formation could also contribute to the lower disk frequency derived from the  $K$  band. Candidate transition disk objects with a mid-infrared excess and  $\Delta K \leq 0.10$  include WSB 18, ISO-Oph 1, WSB 52, ISO-Oph 195, and Object 2-57, SR 21, DoAr 25, SR 9, and WMR 2-37. The latter four have been confirmed as transition disk objects through modeling of their spectral energy distributions from optical through millimeter wavelengths (Eisner et al. 2009; Cieza et al. 2010; Andrews et al. 2011).

#### 4.6.2. Initial Mass Function

Previous investigations of the IMF in  $\rho$  Ophiuchi have produced diverse results. Luhman & Rieke (1999) used  $K$ -band spectra for approximately 100 stars; mass estimates for 36 plus completeness corrections were used to construct an IMF. Their IMF is roughly flat from  $0.05$  to  $1 M_{\odot}$  and peaks at  $\sim 0.4 M_{\odot}$ . de Marchi et al. (2010) use these data and fit it to a tapered power law, and derive a characteristic mass of  $0.17 M_{\odot}$ . Marsh et al. (2010) also derive an IMF for  $\rho$  Ophiuchi which continues to rise into the brown dwarf regime, however this study was completely photometric in nature.

We divided the 123 YSOs that formed an extinction-limited sample ( $A_v \leq 8$  mag) into mass bins with a width in  $\log(\text{mass})$  of 0.4 dex. No correction was made for close binaries. A plot of the resulting mass function, shown in Figure 6, displays a peaks and turns over at  $0.13 M_{\odot}$ .<sup>8</sup> The last three mass bins are

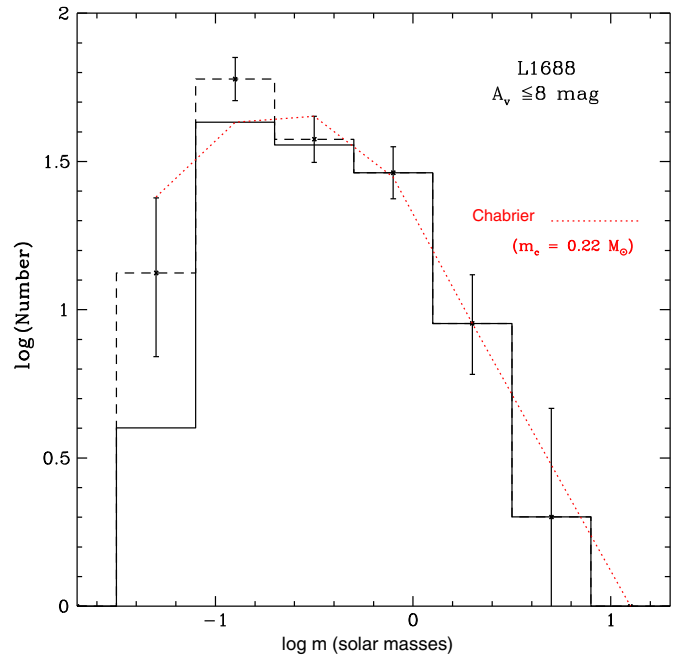


**Figure 6.** Initial mass function for our extinction-limited sample. Dashed lines show the members added from the completeness corrections described in Section 4.6.2. The dotted line is the Chabrier (2003) system mass function which is lognormal for  $M < 1.0 M_{\odot}$  and a power law for  $M > 1.0 M_{\odot}$ . (A color version of this figure is available in the online journal.)

not complete for  $A_v = 8$  mag, so completeness corrections were made assuming an age of 3 Myr. To this end, the maximum visual extinction to which a source could be observed,  $A_{v,\text{max}}$ , was estimated for a source in the center of each mass bin using the DM models and assuming an  $I$ -band limiting magnitude of 15.9. This value, estimated from Figure 2, is where the 3 Myr isochrone intersects our completeness limit. To account for variations in extinction within the region, we used the extinction maps from Ridge et al. (2006) with an effective resolution of  $3'$ . The fractional area of our survey box with  $A_v = 0-2, 2-4, 4-6, 6-8, \text{ and } >8$  mag was estimated to be 0.09, 0.32, 0.24, 0.14, and 0.21, respectively. We then estimated the number of missing sources for each extinction interval assuming a uniform stellar surface density weighted by the fractional area. For the three lowest mass bins, the number of sources would increase by a factor of 1.04, 1.43, and 3.32. While our completeness corrections are dependent on the choice of PMS model and reddening law, the use of other models instead of DM does not significantly change these corrections.

For comparison with our IMF, the lognormal system mass function derived by Chabrier (2003) for field stars with  $M \leq 1.0 M_{\odot}$  is shown in Figure 6 integrated over our mass bins and normalized to the observed number of objects in the  $0.08-0.20 M_{\odot}$  mass bin. For  $M > 1.0 M_{\odot}$ , a power law of the form  $\zeta(\log m) \propto m^{-1.3}$  was used. Error bars plotted in Figure 6 were calculated using the methods of Gehrels (1986) and multiplied by our completeness corrections. In order to make an overall (large scale) comparison of the IMF with other regions and the field star IMF, we computed the ratio of high ( $1-10 M_{\odot}$ ) to low ( $0.1-1 M_{\odot}$ ) mass stars. For our sources, this ratio is  $R = 0.12$  and  $0.10$  when including our completeness corrections with an uncertainty of  $\pm 0.04$  calculated using the methods of Gehrels (1986). Our value of  $R$  is in agreement with values found for  $\rho$  Ophiuchi and other young embedded clusters (Meyer et al.

<sup>8</sup> Objects in mass function with known subarcsecond companions include GSS 5, HD 147889, WLY 2-2, WSB 38, SR 12, SR 9, VSSG 14, SR 24N, ROX 31, SR 20, and SR 13 (see Barsony et al. 2003 and references therein).

2000). The ratio of high-to-low-mass stars for a Chabrier system IMF is 0.16, hence we conclude that coarsely our mass function is consistent with that of the field star IMF. To make a more detailed comparison, a K-S test was performed over the mass ranges for which no completeness corrections were necessary ( $M > 0.2 M_{\odot}$ ). We cannot reject the null hypothesis that the samples were drawn from the same parent population with a probability of 40%, suggesting that the IMF of  $\rho$  Ophiuchi is not significantly different from the field star IMF over this mass range.

When examined in more detail, there might be subtle differences between our mass function and the field star IMF. Chabrier’s (2003) lognormal IMF underestimates the number of objects in the mass bin centered at  $0.13 M_{\odot}$ . In Chabrier (2003), a characteristic mass of  $0.22 M_{\odot}$  was derived for the field star IMF, however we find that our most frequently occurring mass is  $0.13 M_{\odot}$ . Moreover, we note that our lowest mass bin, which is made up of brown dwarfs, has fewer objects than predicted by the model. These differences may be artifacts of methods used to derive our IMF. To quantify the possible deficit, we calculated the ratio of low-mass stars ( $0.08$ – $1 M_{\odot}$ ) to brown dwarfs ( $\leq 0.08 M_{\odot}$ ). Using our completeness-corrected sample, we derive a ratio of  $9.1 (+3.3, -2.6)$  with errors calculated using methods of Gehrels (1986). While this value is within the range found by Andersen et al. (2008) for other star-forming regions, it is higher than values derived for  $\rho$  Ophiuchi by other studies (Geers et al. 2011; Alves de Oliveira et al. 2010). We note that both of these studies were biased toward finding brown dwarfs and only a small subset of their data was confirmed spectroscopically. However, as shown in Figure 6, when the errors in our completeness-corrected values are taken into account, this deficit may not be significant. We conclude that the turnover in our IMF is real, but it is uncertain if there is a real deficit of brown dwarfs compared to the field star IMF. Given the difficulty of estimating completeness corrections for the brown dwarf regime, more sensitive spectroscopic surveys are needed to sample completely this population.

Finally, we compare our IMF to that derived for other star-forming regions, noting that it is dubious to compare directly IMFs which have been derived using different methods. The IMF in the Taurus star-forming cloud differs from most other star-forming regions in that it displays a higher characteristic mass ( $\sim 0.8 M_{\odot}$ ) as well as a corresponding deficit of brown dwarfs (Briceno et al. 2002; Luhman 2004). The IMFs derived for the Orion Nebula Cluster (ONC), IC 348 cluster, and Upper Scorpius are more similar to that in L 1688. While all show a turnover at low mass (Slesnick et al. 2004; Luhman et al. 1998; Slesnick et al. 2008), a somewhat higher characteristic mass of approximately  $0.2 M_{\odot}$  is reported for the ONC and IC 348. Our peak mass of  $0.13 M_{\odot}$  is very similar to that reported by Slesnick et al. (2008) for Upper Scorpius, but unlike our study, they report an *excess* of brown dwarfs relative to the field.

## 5. TEMPORAL RELATIONSHIP WITH UPPER SCO

Given the larger data set for YSOs distributed in the low-extinction regions of the L 1688 cloud, we revisited the relationship between star formation in this extended region ( $6.8 \text{ pc}^2$ ) to that in the L 1688 cloud core and in the Upper Scorpius subgroup of the Sco-Cen OB association. As noted in Paper I and Section 4.5, spectroscopic studies of embedded sources in the  $1 \text{ pc} \times 2 \text{ pc}$  centrally condensed core have consistently yielded ages between 0.1 and 1 Myr when using the D’Antona & Mazzitelli tracks and isochrones, with a median age of 0.3 Myr. The

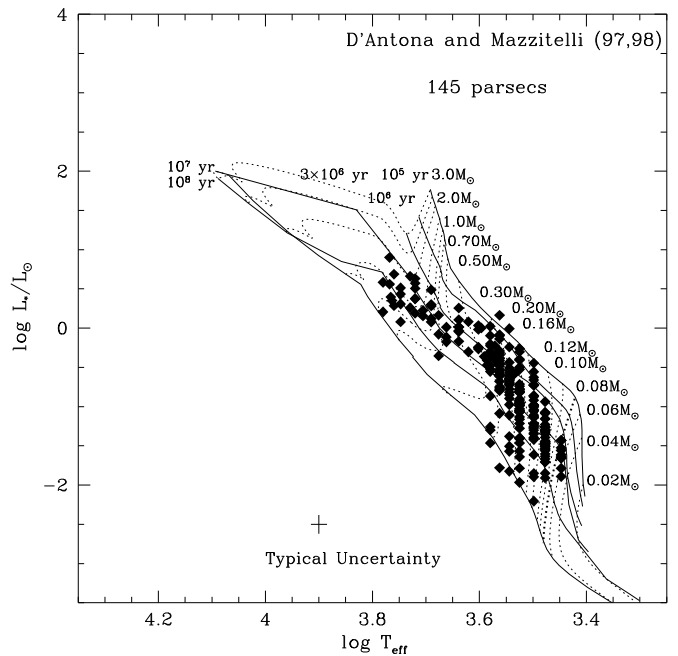


**Figure 7.** Hertzsprung–Russell diagram for 252 low-mass objects in Upper Sco from the study of Preibisch & Zinnecker (1999) relative to the DM97 models. Bolometric luminosities were derived using  $(J-H)$  colors from the 2MASS survey (see the text).

median age for the distributed population is significantly older than that in the higher extinction cloud core.

In Paper I we compared our H-R diagram for 88 association members in L 1688 with that of the 252 members of the Upper Scorpius subgroup compiled by Preibisch et al. (2002) and noted there were no significant differences in age between the two samples. However, comparisons with the Upper Scorpius sample are more complicated since Preibisch et al. derived temperatures and luminosities in a different manner. For example,  $R$ - and  $I$ -band photometry was obtained from the UKST Schmidt plates, intrinsic colors from Hartigan et al. (1994), and the reddening law from Herbig (1998) plus a combination of evolutionary models were used (but primarily those of Palla & Stahler 1999). To ease the comparison between the two samples, we compiled  $(J-H)$  photometry for sources in both samples from the 2MASS catalog (Cutri et al. 2003), transformed it to the CIT system, and derived extinctions and luminosities as described in Section 4.4. A dwarf temperature scale was used to relate spectral types in both samples to effective temperatures. We note that a distance of 130 pc was used for L 1688 and 145 pc for Upper Sco (de Zeeuw et al. 1999). The H-R diagram for the Upper Sco sample is shown in Figure 7 relative to the theoretical tracks and isochrones from D’Antona & Mazzitelli. Ages were interpolated for sources in both samples using the DM models. The average  $\log(\text{age})$  for the Upper Sco sample is 6.43 (2.7 Myr) compared to 6.14 (1.4 Myr) for L 1688. A K-S test applied to both samples suggests that they are not drawn from the same parent population. Hence, in this reanalysis, the low-mass objects distributed across the L 1688 cloud appear intermediate in age between low-mass stars in Upper Sco and YSOs embedded in the centrally condensed core. Consistent with this picture is the lower fraction of K0–M5 stars in Upper Sco with optically thick disks (19%; Carpenter et al. 2006) compared to  $\sim 30\%$  from this study.

Do the timescales involved allow the formation of the distributed population of L 1688 to be triggered by events in Upper

**Table 4**  
Revised Photometry from Paper I

Name	<i>I</i>	( <i>R</i> − <i>I</i> )	Reference
[WMR2005]1 − 29	10.7	1.0	Bouvier & Appenzeller (1992)
[WMR2005]1 − 30	11.57	1.54	S. Gordon & K. M. Strom (1990, private communication)
[WMR2005]1 − 28	11.37	1.17	S. Gordon & K. M. Strom (1990, private communication)
[WMR2005]4 − 66	17.85	...	This study
EM * SR12	10.92	1.27	S. Gordon & K. M. Strom (1990, private communication)
[WMR2005]1 − 26	9.9	0.8	Bouvier & Appenzeller (1992)
[WMR2005]3 − 19	...	...	Edge of image: This study
[WMR2005]1 − 35	11.25	1.45	S. Gordon & K. M. Strom (1990, private communication)
[WMR2005]1 − 15	10.9	1.45	Bouvier & Appenzeller (1992)
[WMR2005]4 − 56	17.04	1.70	This study
[WMR2005]1 − 3	...	...	Saturated: This study

Sco? If a supernova helped power an expanding H I shell originating in Upper Sco and moving at  $\sim 15 \text{ km s}^{-1}$  as proposed by de Geus (1992), then in 1 Myr it would move about 15 pc and barely cover the distance in the plane of the sky between the center of Upper Sco and L 1688. A triggering event from Upper Sco would be consistent with the average age difference of  $\sim 1.3$  Myr between low-mass stars in Upper Sco and L 1688. By retracing the motions of high proper motion objects, Hoogerwerf et al. (2001) suggest that a supernova in a binary system occurred in Upper Sco about 1 Myr ago that produced the runaway star  $\zeta$  Oph and the pulsar PSR J1932+1059. But this would have been too recent for a shock wave to cross the 15 pc expanse between the two regions and initiate the formation of low-mass YSOs in L 1688 with an average age of 2–3 Myr, thus requiring an earlier event.

## 6. SUMMARY

Over 200 moderate resolution optical spectra were obtained for candidate YSOs in a  $1.3 \text{ deg}^2$  area centered on L 1688. When combined with the 136 spectra obtained in our initial spectroscopic study in Paper I, 135 objects with optical spectral types are now identified as association members based on the presence of H $\alpha$  in emission, X-ray emission, lithium absorption, a mid-infrared excess, a common proper motion, reflection nebulosity, or extinction considerations. Fifteen of these display H $\alpha$  in emission consistent with being newly identified CTTS.

Masses and ages were derived for association members using several theoretical models. Using the tracks and isochrones from D’Antona & Mazzitelli (1997) and F. D’Antona & I. Mazzitelli (1998, private communication), we derive an average age of 3.1 Myr for this distributed population. We find a circumstellar disk frequency of  $27\% \pm 5\%$  for our sample, consistent with our derived age and results from other studies. Nine sources are identified as candidate transition disk objects with mid-infrared excesses and no significant *K*-band excess; four of these have been confirmed by recent studies. When compared to simulations, our data are consistent with sampling a single age, artificially spread by uncertainties in the distance, spectral type, and surface gravity suggesting any intrinsic age spread is small. The age of 3.1 Myr for this surface population is intermediate between that of YSOs embedded in the cloud core of  $\rho$  Ophiuchi and low-mass stars in Upper Sco.

We also constructed an IMF for an extinction-limited sample of 123 YSOs ( $A_v \leq 8 \text{ mag}$ ), which is a significant increase in sample size and mass range over previous studies. The resulting IMF is consistent with the field star IMF for YSOs with mass  $> 0.2 M_\odot$ . However, it may be inconsistent for masses below  $0.2 M_\odot$ . We find that our sample has a lower characteristic mass

( $\sim 0.13 M_\odot$ ) than the field star IMF as well as a possible deficit of brown dwarfs.

We are indebted to Tom Greene for offering insightful comments and suggestions. We are very grateful to Lori Allen for assisting with the analysis of data from the *Spitzer Space Telescope*. We also thank John Keller for assistance with the analysis of the Hydra data and the NASA/Missouri Space Grant Consortium for their support. Knut Olsen provided valuable advice on reduction of the CTIO Hydra data. We also thank Francesco Palla for providing a copy of the Palla & Stahler models and Eric Mamajek for a program that interpolates ages and masses from the models. B.W. and K.E. acknowledge support from a grant from the Missouri Research Board and K.E. from a graduate fellowship through the NASA/Missouri Space Grant Consortium. This research has made use of the NASA/IPAC Infrared Science Archive, which is operated by the Jet Propulsion Laboratory, California Institute of Technology, under contract with the National Aeronautics and Space Administration.

## APPENDIX

### PHOTOMETRY REVISED FROM PAPER I

A reanalysis of the *R*- and *I*-band photometry presented in Table 2 of Paper I necessitated some revisions. These revisions, presented in Table 4, are due in large part because of saturation problems with some of the brighter association members. In these cases, photometry was adopted from other studies as noted.

## REFERENCES

- Allen, L. E. 1996, PhD thesis, Univ. Massachusetts  
 Allen, L. E., & Strom, K. M. 1995, *AJ*, **109**, 1379  
 Alves de Oliveira, C., & Casali, M. 2008, *A&A*, **485**, 155  
 Alves de Oliveira, C., Moraux, E., Bouvier, J., et al. 2010, *A&A*, **515**, A75  
 Andersen, M., Meyer, M., Greissl, J., & Aversa, A. 2008, *ApJ*, **683**, L183  
 Andrews, S. M., Wilner, D. J., Espaillat, C., et al. 2011, *ApJ*, **732**, 42  
 Barsony, M., Koresko, C., & Matthews, K. 2003, *ApJ*, **591**, 1064  
 Bastian, N., Covey, K. R., & Meyer, M. R. 2010, *ARA&A*, **48**, 339  
 Bessell, M. S. 1991, *AJ*, **101**, 662  
 Bonnell, I. A., Larson, R. B., & Zinnecker, H. 2007, in *Protostars and Planets V*, ed. B. Reipurth, D. Jewitt, & K. Keil (Tucson, AZ: Univ. Arizona Press), 149  
 Bontemps, S., André, P., Kaas, A., et al. 2001, *A&A*, **372**, 173  
 Bouvier, J., & Appenzeller, I. 1992, *A&AS*, **92**, 481  
 Briceño, C., Luhman, K. L., Hartmann, L., Stauffer, J. R., & Kirkpatrick, J. D. 2002, *ApJ*, **580**, 317  
 Carpenter, J. M. 2001, *AJ*, **121**, 2851  
 Carpenter, J. M., Mamajek, E. E., Hillenbrand, L. A., & Meyer, M. R. 2006, *ApJ*, **651**, L49  
 Casassus, S., Dickinson, C., Cleary, K., et al. 2008, *MNRAS*, **391**, 1075

- Casanova, S., Montmerle, T., Feigelson, E. D., et al. 1995, *ApJ*, **439**, 752
- Chabrier, G. 2003, *PASP*, **115**, 763
- Chini, R. 1981, *A&A*, **99**, 346
- Cieza, L. A., Kessler-Silacci, J. E., Jaffe, D. T., Harvey, P. M., & Evans, N. J., II. 2005, *ApJ*, **635**, 422
- Cieza, L. A., Schreiber, M. R., Romero, G. A., et al. 2010, *ApJ*, **712**, 925
- Cohen, J. G., Frogel, J. A., Persson, S. E., & Elias, J. H. 1981, *ApJ*, **249**, 481
- Cohen, M., & Kuhl, L. V. 1979, *ApJS*, **41**, 743
- Cutri, R. M., et al. 2003, 2MASS All Sky Catalog of Point Sources (The IRSA 2MASS All-Sky Point Source Catalog, NASA/IPAC Infrared Science Archive, <http://irsa.ipac.caltech.edu/applications/Gator/>)
- D'Antona, F., & Mazzitelli, I. 1997, *Mem. Soc. Astron. Ital.*, **68**, 807
- Dahn, C., et al. 2002, *AJ*, **124**, 1170
- de Geus, E. J. 1992, *A&A*, **262**, 258
- de Marchi, G., Paresce, F., & Portegies Zwart, S. 2010, *ApJ*, **718**, 105
- de Zeeuw, P. T., Hoogerwerf, R., Bruijne, J. H. J., Brown, A. G. A., & Blaauw, A. 1999, *AJ*, **117**, 354
- Dolidze, M. V., & Arakelyan, M. A. 1959, *Soviet Astron.*, **3**, 434
- Drilling, J. S., & Landolt, A. U. 2000, in *Astrophysical Quantities*, ed. A. Cox (4th ed.; Melville, NY: AIP), 381
- Eisner, J. A., Monnier, J. D., Tuthill, P., & Lacour, S. 2009, *ApJ*, **698**, L169
- Elias, J. H. 1978, *ApJ*, **224**, 453
- Evans, N. J., II, Dunham, M. M., Jorgenson, J. K., et al. 2009, *ApJS*, **181**, 321
- Fernie, J. D. 1983, *PASP*, **95**, 782
- Gagné, M., Skinner, S., & Daniel, K. 2004, *ApJ*, **613**, 393
- Geers, V. C., Pontoppidan, K. M., van Dishoeck, E., et al. 2007, *A&A*, **476**, 279
- Geers, V. C., Scholz, A., Jayawardhana, R., et al. 2011, *ApJ*, **726**, 23
- Gehrels, N. 1986, *ApJ*, **303**, 336
- Grasdalen, G. L., Strom, K. M., & Strom, S. E. 1973, *ApJ*, **184**, L53
- Greene, T. P., & Meyer, M. R. 1995, *ApJ*, **450**, 233
- Greene, T. P., Wilking, B. A., André, Ph., Young, E. T., & Lada, C. J. 1994, *ApJ*, **434**, 614
- Greene, T. P., & Young, E. T. 1992, *ApJ*, **395**, 516
- Grosso, N., Montmerle, T., Bontemps, S., André, Ph., & Feigelson, E. 2000, *A&A*, **359**, 113
- Haisch, K. E., Lada, E. A., & Lada, C. J. 2000, *AJ*, **120**, 1396
- Hartigan, P., Strom, K. M., & Strom, S. E. 1994, *ApJ*, **427**, 961
- Hartmann, L. 2001, *AJ*, **121**, 1030
- Hawley, S., et al. 2002, *AJ*, **123**, 3409
- Herbig, G. 1998, *ApJ*, **497**, 736
- Herbig, G. H., & Bell, K. R. 1988, *Third Catalog of Emission-Line Stars of the Orion Population* (Lick Obs. Bull. No. 1111; Santa Cruz, CA: Lick Observatory)
- Herbst, W. 2008, in *Handbook of Star Forming Regions Vol. I*, ed. B. Reipurth (San Francisco, CA: ASP), 372
- Hillenbrand, L. A. 2009, in *IAU Symp. 258, The Ages of Stars*, ed. E. E. Mamajek, D. R. Soderblom, & R. Wyse (Cambridge: Cambridge Univ. Press), 81
- Hoogerwerf, R., de Bruijne, J. H. J., & de Zeeuw, P. T. 2001, *A&A*, **365**, 49
- Houk, N., & Smith-Moore, M. 1988, *Michigan Catalogue of Two-dimensional Spectral Types for the HD Stars*, Vol. 4 (Ann Arbor, MI: Univ. Michigan)
- Howell, S. B. 1989, *PASP*, **101**, 616
- Imanishi, K., Koyama, K., & Tsuboi, Y. 2001, *ApJ*, **557**, 747
- Kirkpatrick, J. D., Henry, T. J., & McCarthy, D. W. 1991, *ApJS*, **77**, 417
- Lada, C. J., Muench, A. A., Luhman, K. L., et al. 2006, *AJ*, **131**, 1574
- Landolt, A. U. 1992, *AJ*, **104**, 340
- Loren, R. B. 1989, *ApJ*, **338**, 925
- Luhman, K. L. 2004, *ApJ*, **617**, 1216
- Luhman, K. L., & Rieke, G. H. 1999, *ApJ*, **525**, 440
- Luhman, K. L., Rieke, G. H., Lada, C. J., & Lada, E. A. 1998, *ApJ*, **508**, 347
- Luhman, K. L., Stauffer, J. R., Muench, A. A., et al. 2003, *ApJ*, **593**, 1093
- Mamajek, E. 2008, *Astron. Nachr.*, **329**, 10
- Mamajek, E., Plavchan, P., Kirkpatrick, J., et al. 2010, *ApJ*, **719**, 550
- Martín, E. L., Montmerle, T., Gregorio-Hetem, J., & Casanova, S. 1998, *MNRAS*, **300**, 733
- McClure, M. K., Furlan, E., Manoj, P., et al. 2010, *ApJS*, **188**, 75
- Meyer, M. R., Adams, F. C., Hillenbrand, L. A., Carpenter, J. M., & Larson, R. B. 2000, in *Protostars and Planets IV*, ed. V. Mannings, A. P. Boss, & S. Russell (Tucson, AZ: Univ. Arizona Press), 121
- Meyer, M. R., Calvet, N., & Hillenbrand, L. A. 1997, *AJ*, **114**, 288
- Montmerle, T., Koch-Miramonde, L., Falgarone, E., et al. 1983, *ApJ*, **269**, 182
- Natta, A., Testi, L., Comerón, F., et al. 2002, *A&A*, **393**, 597
- Ozawa, H., Grosso, N., & Montmerle, T. 2005, *A&A*, **429**, 963
- Palla, F., & Stahler, S. W. 1999, *ApJ*, **525**, 772
- Prato, L. 2007, *ApJ*, **657**, 338
- Preibisch, T., Brown, A. G. A., Bridges, T., Guenther, E., & Zinnecker, H. 2002, *AJ*, **124**, 404
- Preibisch, T., & Zinnecker, H. 1999, *AJ*, **117**, 2381
- Ridge, N. A., Di Francesco, J., Kirk, H., et al. 2006, *AJ*, **131**, 2921
- Schmidt-Kaler, Th. 1982, in *Landolt-Bornstein New Series, Numerical Data and Functional Relationships in Science and Technology, Group 4, Vol. 2b*, ed. K. Schaffers & H. H. Voigt (New York: Springer), 451
- Siess, L., Dufour, E., & Forestini, M. 2000, *A&A*, **358**, 593
- Skrutskie, M. F., et al. 1990, *AJ*, **99**, 1187
- Slesnick, C. L., Hillenbrand, L. A., & Carpenter, J. M. 2004, *ApJ*, **610**, 1045
- Slesnick, C. L., Hillenbrand, L. A., & Carpenter, J. M. 2008, *ApJ*, **688**, 377
- Struve, O., & Rudkjobing, M. 1949, *ApJ*, **109**, 92
- Torres, C. A. O., Quast, G. R., da Silva, L., et al. 2006, *A&A*, **460**, 695
- Vrba, F. J., Strom, K. M., Strom, S. E., et al. 1975, *ApJ*, **197**, 77
- Vrba, F. J., Strom, S. E., & Strom, K. M. 1976, *AJ*, **81**, 958
- Walter, F. M., et al. 1994, *AJ*, **107**, 692
- Wilking, B. A., Gagné, M., & Allen, L. E. 2008, in *Handbook of Star Forming Regions Vol. II*, ed. B. Reipurth (San Francisco, CA: ASP), 351
- Wilking, B. A., & Lada, C. J. 1983, *ApJ*, **274**, 698
- Wilking, B. A., Lada, C. J., & Young, E. T. 1989, *ApJ*, **340**, 823
- Wilking, B. A., Meyer, M. R., Robinson, J. G., & Greene, T. P. 2005, *AJ*, **130**, 1733 (Paper I)
- Wilking, B. A., Schwartz, R. D., & Blackwell, J. H. 1987, *AJ*, **94**, 106
- Wilking, B. A., Schwartz, R. D., Fanetti, T., & Friel, E. 1997, *PASP*, **109**, 549
- Zacharias, N., Finch, C., Girard, T., et al. 2009, *VizieR On-line Data Catalog: I/315*